(2)

AD-A221 407

AD No. _____

TECOM Project No. 7-CO-R89-DPO-010

DPG No. DPG-FR-90-705

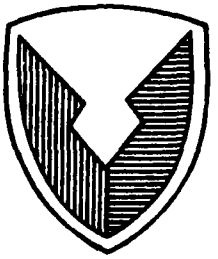

US ARMY
MATERIEL COMMAND

METHODOLOGY INVESTIGATION

FINAL REPORT

CALIBRATION AND QUALITY CONTROL FOR NEW METEOROLOGICAL INSTRUMENTATION, PART I

By

CHRISTOPHER A. BILTOFT

Meteorology Division
Materiel Test Directorate

U.S. ARMY DUGWAY PROVING GROUND
DUGWAY, UTAH 84022-5000

NOVEMBER 1989

Period Covered:
October 1988-September 1989

Distribution unlimited.

Prepared for:
Commander, U.S. Army Test and Evaluation command, ATTN: AMSTE-AD-M, Aberdeen Proving Ground, MD 21005-5055

U.S. Army Test and Evaluation Command, Aberdeen Proving Ground, MD 21005-5055

Disposition Instructions

Destroy this report when no longer needed. Do not return it to the originator.

Disclaimer Statement

The views, opinions, and findings in this report are those of the authors and should not be construed as an official Department of the Army position, unless so designated by other official documentation.

Trade Name Statement

The use of trade names in this report does not constitute an official endorsement or approval of the use of such commercial hardware or software. This report may not be cited for purposes of advertisement.

DEPARTMENT OF THE ARMY
HEADQUARTERS, U.S. ARMY TEST AND EVALUATION COMMAND
ABERDEEN PROVING GROUND, MARYLAND 21005-5055

REPLY TO
ATTENTION OF

2 MAR 1990

AMSTE-TC-M (70-10p)

MEMORANDUM FOR Commander, U.S. Army Dugway Proving Ground, ATTN: STEDP-MT-M, Dugway, UT 84022-5000

SUBJECT: Final Report: Calibration and Quality Control for New Meteorological Instrumentation, Part I, TECOM Project No. 7-CO-R89-DPO-010

1. Subject report is approved.

2. Point of contact at this headquarters is Mr. James Piro, AMSTE-TC-M, amstetcm@apg-emh4.apg.army.mil, AUTOVON 298-2170.

FOR THE COMMANDER:

Grover H. Shelton

GROVER H. SHELTON
Chief, Meth Imprv Div
Directorate for Technology

UNCLASSIFIED
SECURITY CLASSIFICATION OF THIS PAGE

REPORT DOCUMENTATION PAGE

Form Approved OMB No. 0704-0188

1a. REPORT SECURITY CLASSIFICATION UNCLASSIFIED	1b. RESTRICTIVE MARKINGS
2a. SECURITY CLASSIFICATION AUTHORITY	3. DISTRIBUTION/AVAILABILITY OF REPORT Approved for Public Release; Distribution Unlimited
2b. DECLASSIFICATION/DOWNGRADING SCHEDULE	
4. PERFORMING ORGANIZATION REPORT NUMBER(S) DPG-FR-90-705	5. MONITORING ORGANIZATION REPORT NUMBER(S)
6a. NAME OF PERFORMING ORGANIZATION U.S. Army Dugway Proving Ground 6b. OFFICE SYMBOL (If applicable) STEDP-MT-M	7a. NAME OF MONITORING ORGANIZATION
6c. ADDRESS (City, State, and ZIP Code) Dugway, UT 84022-5000	7b. ADDRESS (City, State, and ZIP Code)
8a. NAME OF FUNDING/SPONSORING ORGANIZATION U.S. Army Test and Evaluation Command 8b. OFFICE SYMBOL (If applicable) AMSTE-AD-M	9. PROCUREMENT INSTRUMENT IDENTIFICATION NUMBER
8c. ADDRESS (City, State, and ZIP Code) Aberdeen Proving Ground, MD 21005-5055	10. SOURCE OF FUNDING NUMBERS PROGRAM ELEMENT NO. / PROJECT NO. 7-CO-R89-DPO-010 / TASK NO. / WORK UNIT ACCESSION NO.

11. TITLE (Include Security Classification)
Calibration and Quality Control for New Meteorological Instrumentation, Part I

12. PERSONAL AUTHOR(S)
Biltoft, Christopher A.

13a. TYPE OF REPORT	13b. TIME COVERED	14. DATE OF REPORT (Year, Month, Day)	15. PAGE COUNT
Methodology Report	FROM Oct 88 TO Sep 89	1989, November, 15	

16. SUPPLEMENTARY NOTATION

17. COSATI CODES			18. SUBJECT TERMS (Continue on reverse if necessary and identify by block number)		
FIELD	GROUP	SUB-GROUP	anemometer	Doppler Acoustic Sounder	remote sensing
04	02		ASTM	Intercomparison Testing	scintillometer
			calibration	quality control	sodar

19. ABSTRACT (Continue on reverse if necessary and identify by block number)

U.S. Army Dugway Proving Ground (DPG) conducted tests to verify performance and develop quality control procedures for new meteorological instrumentation. The instrumentation tested included cup and sonic anemometers, Doppler acoustic sounders (sodars), and a crosswind scintillometer. Sonic anemometer intercomparison tests conducted at the Boulder Atmospheric Observatory (BAO) identified deficiencies in the DPG sonic anemometer software. These deficiencies are being corrected by the manufacturer. The sonic anemometer transducer shadow correction algorithm was characterized in a low turbulence wind tunnel. It's response in turbulent flow was then compared to the response of cup anemometers. These tests verified the sonic anemometer's transducer shadow correction algorithm. A novel means of evaluating cup anemometer overspeeding was developed from cup versus sonic anemometer intercomparisons. With data processing differences and overspeed effects removed,
(Cont'd on next page)

20. DISTRIBUTION/AVAILABILITY OF ABSTRACT	21. ABSTRACT SECURITY CLASSIFICATION
☒ UNCLASSIFIED/UNLIMITED ☐ SAME AS RPT. ☐ DTIC USERS	UNCLASSIFIED

22a. NAME OF RESPONSIBLE INDIVIDUAL	22b. TELEPHONE (Include Area Code)	22c. OFFICE SYMBOL
Christopher A. Biltoft	(801)831-5101	STEDP-MT-M

DD Form 1473, JUN 86 *Previous editions are obsolete.*

SECURITY CLASSIFICATION OF THIS PAGE
UNCLASSIFIED

19. ABSTRACT (CONT'D)
cup and sonic anemometer mean wind measurements were shown to be essentially equivalent. Two draft ASTM documents, one addressing sonic anemometer measurement practices and the other addressing performance testing, were prepared for ASTM committee review. A DPG sodar participated in the International Sodar Intercomparison Experiment (ISIE) at the BAO. Preliminary ISIE results indicate that sodars provide reliable wind speed and direction profile measurements during low to moderate wind speeds. Sodar data can be used for first-order approximations of boundary layer vertical velocity variance, but sodars do not generate reliable horizontal wind angle standard deviation data. A crosswind scintillometer weighting function verification study was conducted at DPG. Data from this test are awaiting analysis.

TABLE OF CONTENTS

FOREWORD

This project was partially supported by FY89 Research, Development, Test, and Evaluation (RDTE) methodology funds. The study was performed by the Meteorology Division, Materiel Test Directorate, U.S. Army Dugway Proving Ground. Other participants included John Gaynor and Norbert Szczepczynski of the National Oceanic and Atmospheric Administration (NOAA) Environmental Research Laboratories/Wave Propagation Laboratory (ERL/WPL) who assisted with the collection and analysis of data for the Sonic Anemometer Intercomparison Experiment. Mr. Gaynor and Dr. Bruce Baker of the U.S. Environmental Protection Agency (EPA) Research Triangle Park Office were the co-principal organizers of the International Sodar Intercomparison Experiment (ISIE). Dr. Baker also performed the sonic anemometer wind tunnel characterization referenced in this report. Data collection for the Crosswind Scintillometer Study and the Light Tunnel Study was performed by Mr. James Osterud of the Dugway Instrumentation Branch, Test Data Division. Mrs. Susan Gross provided word processing support during report preparation. Mr. James Bowers, Chief of the Dugway Meteorology Division, and Mr. Thomas Lockhart of Meteorological Standards Institute provided invaluable consultation in the preparation of the the Light Tunnel Study.

SECTION 1. SUMMARY

1.1 BACKGROUND

U.S. Army Dugway Proving Ground (DPG) has acquired a number of new meteorological instruments over the past several years that offer measurement capabilities unavailable with older instrument designs. Some of these systems such as the Doppler acoustic sounder (sodar) and the scintillometer are remote sensing instruments that require extensive intercomparison testing to determine their performance. Other instruments such as the sonic anemometers can be characterized in a wind tunnel, but require intercomparison testing in the ambient atmosphere or some other turbulent environment.

This Part I study reports on the FY89 DPG contribution to the international effort to develop meteorological applications for emerging remote sensing technologies. This effort is important to the Department of Defense test and evaluation community because of increasing demands for the specification of atmospheric effects on multispectral target acquisition systems, smokes/obscurants, and munitions delivery systems. The Sonic Anemometer Intercomparison Study and the International Sodar Intercomparison Experiment (ISIE) were collaborative efforts conducted at the Boulder Atmospheric Observatory (BAO). Other participants in the ISIE included the National Oceanic and Atmospheric Administration (NOAA) Environmental Research Laboratories/Wave Propagation Laboratory (ERL/WPL) and the U.S. Environmental Protection Agency (EPA). The ISIE also included participants from France and Japan, with observers from several other nations. The Crosswind Scintillometer Weighting Function Test and the Light Tunnel Anemometer Studies were conducted at DPG with in-house resources.

1.2 PROBLEM

Before fielding DPG's new meteorological instruments, it is necessary to verify their performance through calibration checks and field studies, and to develop procedures for processing and interpreting the ensuing data.

1.3 OBJECTIVE

The objective of this study was to characterize the performance of new meteorological instrument systems, define procedures for their operation, and test data reduction and analysis procedures.

1.4 PROCEDURES

The emphasis of the Part I study was placed on the sonic anemometers because they are urgently needed to replace existing mechanical wind sensors. Sonic anemometers provide the detailed wind and turbulence data needed to define the state of the surface boundary layer. They also serve as a field reference for performance tests of other instruments. Other instrumentation used in this study included sodars, crosswind scintillometers, and the cup anemometers currently used for micrometeorological wind measurements.

The sonic anemometer consists of paired sets of acoustic transmitters and receivers, with a system clock and microprocessor circuitry to count intervals of time between transmission and reception of sound pulses. An orthogonal coplanar acoustic array measures horizontal wind components, and a third axis

oriented in the vertical plane measures vertical wind components. The fundamental measurement unit is the transit time of acoustic pulses between transmitter/receiver pairs. Transit time, with a known transit distance or pathlength, provides an along-axis velocity component. The output of the sonic anemometer consists of measurements of near-instantaneous wind components along the three orthogonal axes at a 10-Hz sampling rate. The along-axis wind data are transformed by external software to wind speed, wind direction, and turbulence intensity. Further details on sonic anemometers are found in the report "Development of Sonic Anemometer Software" by Biltoft (1987).

The crosswind scintillometer consists of transmitter and receiver optics and accompanying electronics mounted within water resistant cases. Crosswind measurements are made along an optical path defined between the transmitter and receiver. The transmitter uses a Light Emitting Diode (LED) source radiating over Fresnel lenses, and the receiver optics contain another set of Fresnel lenses. Alternating clear and reflecting stripes on the lenses form zero-mean filters of 5-, 10-, and 20-cm wavelengths. Combinations of the transmitter and receiver filters define spatial filters that are sensitive to cross-path wind components at segments along the optical path. The filter combinations selected for this instrument form weighting functions with maximum sensitivity to the crosswinds at the 1/5, 1/3, 1/2, 2/3, and 4/5 path segments. This instrument is therefore capable of providing simultaneous wind component readings at five segments along an optical path. The total path length is user selectable and can range from 300 to 1500 m. Further details and initial test results on the crosswind scintillometer are provided in "Field Test of a Crosswind Scintillometer" by Biltoft (1988).

Sodars are ground-based remote sensing devices that use the Doppler effect to measure vertical profiles of wind and turbulence in the atmospheric boundary layer. Acoustic pulses are transmitted from compression drivers within tuned directional antennas. These antennas direct the acoustic energy along the vertical axis and axes tilted towards the north or south and east or west. Thermal inhomogeneities in the atmosphere scatter the acoustic energy, and the receiver horns collect the backscattered component of the signal. The return signal is characterized by its intensity and Doppler frequency shift. The Doppler shift is towards higher frequency if air in the scattering volume is moving towards the antenna and towards a lower frequency if the scattering volume is moving away from the antenna. System algorithms are used to convert Doppler shift data into horizontal and vertical wind velocity components. Sodars typically provide 15-min averaged vertical wind profiles between 50 to 600 m with a range resolution of 25 to 50 m. Initial sodar performance test results are presented in "Intercomparison of Wind Measurements from Two Acoustic Doppler Sodars, a Laser Doppler Lidar, and In Situ Sensors" by Chintawongvanich et al. (1989).

1.5 RESULTS

As noted above, the major effort of the Part I study was expended on the sonic anemometer. A series of intercomparison tests were conducted at BAO using three types of sonic anemometer, including the DPG model, mounted in close proximity. The test results showed that these sonic anemometers produce precise wind and turbulence measurements. Discrepancies noted in the data from the DPG sonic anemometer were determined to be due to sampling algorithm deficiencies. The problem was brought to the attention of the manufacturer,

who corrected the problem and is installing updated software in the DPG units at no cost to the government. Follow-on tests using the corrected software have confirmed that the problem has been resolved. The follow-on test results are being prepared for publication in a paper entitled "Minimizing Flow Distortion Errors in a Sonic Anemometer" by Kaimal et al.

The sonic anemometer was also evaluated as a means of making fast response temperature measurements. With a minor change in data processing software, a speed of sound output was obtained for the vertical axis and converted to virtual temperature. The BAO tests results were very satisfactory, and the DPG three-axis sonic anemometers are being programmed to output virtual temperature for use in temperature flux computations. Initial results are presented in the Sonic Anemometer Intercomparison Study section of this report, and a more detailed report on these results will appear in the flow distortion error paper by Kaimal et al.

One DPG sonic anemometer was sent to Dr. Bruce Baker at the EPA Research Triangle Park Offices for extensive characterization in the EPA wind tunnel. Dr. Baker found that, under laminar flow conditions, the transducer shadow compensation algorithm has velocity and wind-angle dependencies that produce uncertainties of 3 to 5 percent in absolute wind velocity measurements. However, studies of this phenomenon conducted in turbulent flow at the Dugway Light Tunnel failed to find evidence of these angular dependencies. The differences in the results for laminar and turbulent flows are believed to be explained by turbulent mixing, which probably disperses transducer wake effects and thus minimizes measurement uncertainty. This issue is also addressed in the flow distortion error paper being prepared by Kaimal et al.

The DPG Light Tunnel study also collected data to characterize the performance of the DPG cup anemometers in terms of turbulence scale and intensity, and a novel cup anemometer overspeed estimation technique was developed. This technique provided overspeed estimates of 5 percent for the DPG fast response cup anemometers. The Light Tunnel study also identified the need to measure cup anemometer distance constants during both spin up and spin down. A detailed report on the Light Tunnel study is in Appendix B.

Information gained during the BAO Intercomparison, EPA wind tunnel, and DPG Light Tunnel studies were used to prepare drafts of two American Society for the Testing of Materials (ASTM) documents. The first document ("A Standard Practice for Measuring Surface Wind and/or Temperature by Sonic Means"), which is a guide for sonic anemometer users, addresses deployment, data reduction algorithms, interferences, calibration, and quality control. The second document ("A Standard Test Method for Determining the Performance of a Sonic Anemometer/Thermometer") is a detailed set of procedures for use by manufacturers and testing laboratories to characterize the various models of sonic anemometers. Both draft documents have been submitted for review by ASTM Committee D22.11 on The Sampling of Atmospheres/Meteorology. The two draft ASTM documents are in Appendices C and D.

Data from the International Sodar Intercomparison Experiment (ISIE) were reduced and exchanged with other participants. The results of initial analyses indicate that the sodars are useful for profiling wind speed and direction when certain atmospheric conditions prevail. For example, 20-min averaged profiles of wind speed and direction compared well with those obtained from the BAO

tower when wind speeds were 8 m/s or less. The initial results also indicate that sodar vertical velocity variance data should be used with caution. For extremely unstable atmospheric conditions with a horizontally inhomogeneous atmosphere, the vertical velocity variance can be in error due to the lack of a common sampling volume for the three antennas. Sodar vertical velocity variances can also be unrepresentative during stable nocturnal conditions because of the sodar's slow pulse repetition frequency. None of the tested sodars was able to provide satisfactory estimates of horizontal wind angle standard deviations.

1.6 CONCLUSIONS

Sonic anemometers are now the most extensively tested and completely characterized fast response instruments available for field use. Their inertia-free response to the turbulent wind field and short pathlength provide wind and turbulence measurement capabilities unequaled by other available field instruments. Sonic anemometers can also provide the fast-response temperature measurements needed for heat flux computation. On the other hand, biases may appear in the data due to uncompensated transducer shadow effects, and the transducer array must be precisely aligned and leveled in order to achieve high measurement accuracy. Sonic anemometer transducers are also sensitive to noise. The transducers are tiny microphones, and field experience has shown that they will pick up extraneous noise. As a rule of thumb, sonic anemometers should be mounted at a height where the wavelength of the spectral peak in atmospheric turbulence exceeds the instrument's pathlength by a factor of 2π or more. Over flat, open terrain, a sonic anemometer with a 15-cm path should provide reasonable wind component and turbulence measurements at or above the 2-m level.

The cup anemometer's strength lies in its ruggedness, simplicity, ease of wind tunnel calibration, and unobstructed exposure to horizontal wind components. Cup anemometers overspeed in turbulent flow when vertical motions are present. Thus, cup anemometer mean wind speeds should be corrected for overspeeding if highly accurate wind measurements are needed. To minimize overspeed effects, cup anemometers should be mounted at a height where the wavelength of the turbulence spectral peak exceeds the instrument's distance constant by a factor of 4π or more. However, a cup anemometer so mounted will still overspeed in response to vertical motions. Cup anemometer distance constants for both spin up and spin down are needed to define the mean distance constant.

Major differences between cup and sonic anemometer wind readings arise from data reduction algorithms. Cup anemometers usually provide scalar measurements, while sonic anemometer velocity component measurements are usually converted to vector winds. A scalar wind computation algorithm developed for the sonic anemometer removes most of the measurement differences. If a cup anemometer's overspeed effects are also removed from the data, mean wind-speed measurement differences between the cup and sonic anemometer are within the instruments' measurement uncertainties.

Sodars are currently the best commercially available instruments for wind-speed and direction profile measurements within the boundary layer. Sodar data reliability increases with averaging time, with optimum averaging periods of 15 to 30 min. Sodar vertical velocity variance data can be used to provide first-

order turbulence estimates. However, the sodar's slow pulse repetition rate and volume averaging limit its accuracy during very stable or very unstable conditions. Also, sodars cannot provide reliable estimates of horizontal wind angle standard deviations.

1.7 RECOMMENDATIONS

Sonic anemometers should become the primary source of wind data on DPG tests requiring detailed wind, flux, and turbulence information. This recommendation cannot be implemented until DPG receives its new digital data collection system, which is designed to collect, process, and display both digital and analog data. Cup anemometers can be used for mean scalar wind measurements in low turbulence conditions, but should be corrected for over-speeding if otherwise employed. Uncorrected cup anemometer data should not be used for surface boundary layer wind speed profile measurements. Sodars are acceptable for mean wind profile measurements. Sodar vertical turbulence component measurements provide first-order estimates of the boundary layer's vertical turbulence structure, but the sodar's horizontal wind variance data are too unreliable for use as test data.

INTENTIONALLY BLANK

SECTION 2. DETAILS OF THE TEST

2.1 THE SONIC ANEMOMETER INTERCOMPARISON TEST

The sonic anemometer intercomparison study was conducted at the BAO near Erie, Colorado. The BAO is an atmospheric boundary layer research facility featuring an instrumented 300-m tower located on gently rolling terrain 25 km east of Boulder, Colorado. The BAO is operated by the NOAA ERL/WPL to support boundary layer studies and instrument development and testing. Additional BAO site information is provided by Kaimal and Gaynor (1983).

Three sonic anemometers were mounted at 22 m on the BAO tower's carriage platform with an orientation of 224 deg during the Sonic Anemometer Intercomparison Test. The BAO research-grade sonic anemometer was mounted in the middle of the carriage. The "Kaimal-head" (hereafter designated as KAI) and the DPG 15-cm units were mounted on either side with a spacing of 1 m between anemometers. The KAI differs from the DPG unit in that the v-component axis is rotated under the support arm rather than being coplanar with the u-component axis. This unit also a has slightly smaller support structure and updated software. Both the KAI and DPG sonic anemometers have 15-cm acoustic pathlengths and use an inverse time solution to derive wind and temperature data (see Biltoft, 1987). The BAO research grade sonic anemometer has 25-cm paths on its three axes and uses a direct time solution for wind component measurement only. It's temperature is obtained from a fast-response platinum wire resistance temperature device (RTD) mounted within the vertical axis. All three sonic anemometers operate at 200 Hz, averaging 20 returns to produce each 10-Hz data point. The BAO research grade sonic anemometer was used as the reference instrument for the intercomparison trials.

Sonic anemometer intercomparison tests were conducted on 9 August 1988 with moderate to strong southwesterly wind providing favorable exposure for all three anemometer arrays. One test was conducted during midday convective conditions, and the the other during the evening transition to nocturnal conditions. Several hours of data were collected for each period. All instruments were calibrated prior to use.

The presence of three sonic anemometers permitted a 3-way intercomparison of results. Comparisons were done using as figures of merit the bias (β), comparability (χ), precision (π), and normalized precision (π') as defined by Hoehne (1971) and recommended by ASTM D 4430-84, "Standard Practice for Determining the Operational Comparability of Meteorological Measurements." Three sets of differences were calculated using $X_{ai}-X_{bi}$, $X_{bi}-X_{ci}$, and $X_{ai}-X_{ci}$, where X represents a measurement made by instrument a, b, or c. The expressions for β, χ, π, and π' are

$$\beta = \frac{1}{N}\sum_{i=1}^{N}(X_{ai}-X_{bi}) \qquad (1)$$

$$\chi = \left[\frac{1}{N} \sum_{i=1}^{N} (X_{ai} - X_{bi})^2 \right]^{1/2} \tag{2}$$

$$\pi = [N(\chi^2 - \beta^2)/(N-1)]^{1/2} \tag{3}$$

$$\pi' = 100 \left[\frac{s}{X_{BAO}} \right] \tag{4}$$

where

X_{ai} = wind component measurement made by anemometer a for the ith time period

X_{bi} = wind component measurement made by anemometer b for the ith time period

N = the number of samples

X_{BAO} = mean wind component measured by the BAO sonic anemometer

Bias is the average difference between the anemometers, χ is the root mean square difference with bias included, precision is the standard deviation of these differences, and π' expresses precision as a percentage of the variable measured by the BAO sonic anemometer. The intercomparison test results for convective and transition to stable conditions are given in Tables 1 and 2, respectively.

Relatively large biases were observed in the mean velocities and the alongwind and crosswind velocity variances obtained by the DPG sonic anemometer. These effects are especially noticeable for the transition trial data in Table 2. These data were collected as atmospheric motions became more stratified due to the cessation of the convectively driven turbulent mixing. The biases were due in part to a 3-deg orientation angle difference between the DPG and BAO sonic anemometers. Extreme measurement accuracies can be achieved with sonic anemometers only if the instruments are precisely aligned and leveled.

The intercomparison trials surfaced several deficiencies in the DPG sonic anemometer software. The first is grab sampling at the beginning of each 0.1-s measurement period instead of sampling at equal intervals throughout the period. The second deficiency is in the auto-calibration technique, which uses an insufficient sample size to be representative of average atmospheric conditions. Even with the orientation and software problems, the normalized precisions of 1 or 2 percent between the DPG and BAO sonic anemometers are better than precisions achievable using mechanical anemometers in the turbulent atmosphere.

Table 1. Bias, Comparability, Precision, and Normalized Precision for the Convective Sonic Anemometer Intercomparison Trials, 9 August 1988 1520-1700 MDT.

Variable	Instrument	Bias (MKS Units) β	Comparability (MKS Units) χ	Precision (MKS Units) π	Normalized Precision π'
Mean	BAO-DPG	-0.042	0.063	0.050	1.0
Velocity	DPG-KAI	0.038	0.053	0.041	0.9
($\bar{u}$)	BAO-KAI	-0.004	0.029	0.031	0.7
Alongwind	BAO-DPG	-0.160	0.167	0.050	5.0
Variance	DPG-KAI	0.070	0.072	0.019	1.9
($\overline{u'u'}$)	BAO-KAI	-0.091	0.097	0.035	3.4
Crosswind	BAO-DPG	0.045	0.075	0.064	5.7
Variance	DPG-KAI	-0.093	0.139	0.111	10.0
($\overline{v'v'}$)	BAO-KAI	-0.048	0.068	0.051	4.6
Vertical	BAO-DPG	-0.009	0.011	0.007	2.1
Variance	DPG-KAI	-0.009	0.015	0.013	4.0
($\overline{w'w'}$)	BAO-KAI	-0.018	0.022	0.014	4.2
Temperature	BAO-DPG	0.011	0.020	0.018	14.2
Variance	DPG-KAI	-0.008	0.016	0.015	11.9
($\overline{T'T'}$)	BAO-KAI	0.003	0.012	0.012	9.7
Temperature	BAO-DPG	-0.007	0.012	0.010	9.3
Flux	DPG-KAI	-0.004	0.011	0.011	10.0
($\overline{w'T'}$)	BAO-KAI	-0.012	0.012	0.003	3.2
Stress	BAO-DPG	0.010	0.012	0.007	3.5
($\overline{u'w'}$)	DPG-KAI	0.006	0.011	0.010	4.7
	BAO-KAI	0.016	0.019	0.011	4.8

Table 2 Bias, Comparability, Precision, and Normalized Precision for the Transition Sonic Anemometer Intercomparison Trials, 9 August 1988 2030-2150 MDT.

Variable	Instrument	Bias (MKS Units) β	Comparability (MKS Units) χ	Precision (MKS Units) π	Normalized Precision π'
Mean	BAO-DPG	-0.278	0.309	0.143	2.6
Velocity	DPG-KAI	0.240	0.258	0.103	1.9
($\bar{u}$)	BAO-KAI	-0.039	0.059	0.047	0.9
Alongwind	BAO-DPG	-0.006	0.045	0.048	14.3
Variance	DPG-KAI	0.026	0.054	0.051	15.2
($\overline{u'u'}$)	BAO-KAI	-0.020	0.041	0.038	11.3
Crosswind	BAO-DPG	0.032	0.087	0.087	34.5
Variance	DPG-KAI	-0.029	0.079	0.079	31.3
($\overline{v'v'}$)	BAO-KAI	0.003	0.012	0.013	5.1
Vertical	BAO-DPG	-0.002	0.005	0.005	10.2
Variance	DPG-KAI	0.001	0.006	0.006	12.4
($\overline{w'w'}$)	BAO-KAI	-0.002	0.003	0.002	4.2
Temperature	BAO-DPG	0.022	0.028	0.018	13.9
Variance	DPG-KAI	0.001	0.010	0.011	8.2
($\overline{T'T'}$)	BAO-KAI	0.023	0.027	0.015	11.6
Temperature	BAO-DPG	0.011	0.010	0.005	30.9
Flux	DPG-KAI	-0.012	0.011	0.005	29.4
($\overline{w'T'}$)	BAO-KAI	-0.001	0.003	0.003	16.0
Stress	BAO-DPG	-0.000	0.009	0.010	34.0
($\overline{u'w'}$)	DPG-KAI	-0.003	0.009	0.010	33.3
	BAO-KAI	-0.003	0.004	0.003	11.1

The vertical velocity variance and stress results shown in Tables 1 and 2 are very good, indicating that the vertical axes of all instruments were precisely leveled and properly exposed. Even during the low turbulence transition trials, vertical velocity normalized precisions were on the order of 10 percent. The transition trial stress computations using the DPG sonic anemometer data suffered from the alignment and software problems mentioned above.

The sonic anemometer fast response temperature measurements were highly successful. Computational uncertainties render the absolute temperature measurements unreliable, but the fluctuating components that remain after removal of the mean were found to be sufficiently accurate for temperature flux and variance computations. Thermal inertia effects were observed in the BAO sonic anemometer's RTD when its output was compared to the inertia-free DPG and KAI sonic temperature components. These intercomparison trials conclusively demonstrated the efficacy of sonic temperature measurements for computation of temperature variance and temperature flux.

The Sonic Anemometer Intercomparison Test results identified the need to upgrade the DPG sonic anemometer software. This upgrade is in process and should be completed by the spring of 1990. The most recent test results using upgraded software are being prepared for publication in Boundary Layer Meteorology under the title "Minimizing Flow Distortion Errors in a Sonic Anemometer" (Dr. Chandran Kaimal, personal communication).

2.2 THE INTERNATIONAL SODAR INTERCOMPARISON EXPERIMENT

The International Sodar Intercomparison Experiment (ISIE) was conducted at the BAO from 29 August to 16 September 1988. The purpose of the ISIE was to perform intercomparison testing of commercially available Doppler acoustic sounders (sodars). ISIE data will be used to evaluate sodar performance and to develop an ASTM standard for acoustic remote sensing of wind profiles.

Sodars available for the ISIE included the U.S. AeroVironment and Xontec sodars, the French Remtech sodar, and an experimental phased-array sodar developed by Dr. Ito for the Japanese company Kaijo-Denki. The sodars provided by AeroVironment, Xontec, and Remtech were stationed near the outside anchor points of the BAO tower cables, while the DPG sodar, U.S. Army Atmospheric Sciences Laboratory (ASL) sodar, and the experimental phased-array sodar were clustered near the BAO site entrance. The DPG sodar operated at 2400 Hz and the ASL sodar operated at 1600 Hz. Additional instrumentation present included a NOAA/ERL 3.2 cm radar operated in a velocity-azimuth display (VAD) mode. Data from this radar are not yet available for analysis. The ISIE test results are of particular interest to DPG because, in addition to the DPG-supplied sodar, the Aerovironment (AV) and Remtech (REM) 1600-Hz sodars included in the ISIE are also used at DPG.

With the exception of the DPG unit, all of the sodars were mounted on trailers with their horns clustered in the normal deployment configuration. The DPG sodar was dismounted from its trailer so that the off-vertical horns could be pointed towards the vertical horn. This configuration was used to minimize sampling volume separation. With a spacing of 42 m, this arrangement provided a common measuring volume at 150 m above ground level. Details of the DPG sodar configuration and other nearby instrumentation are shown in Figure 1.

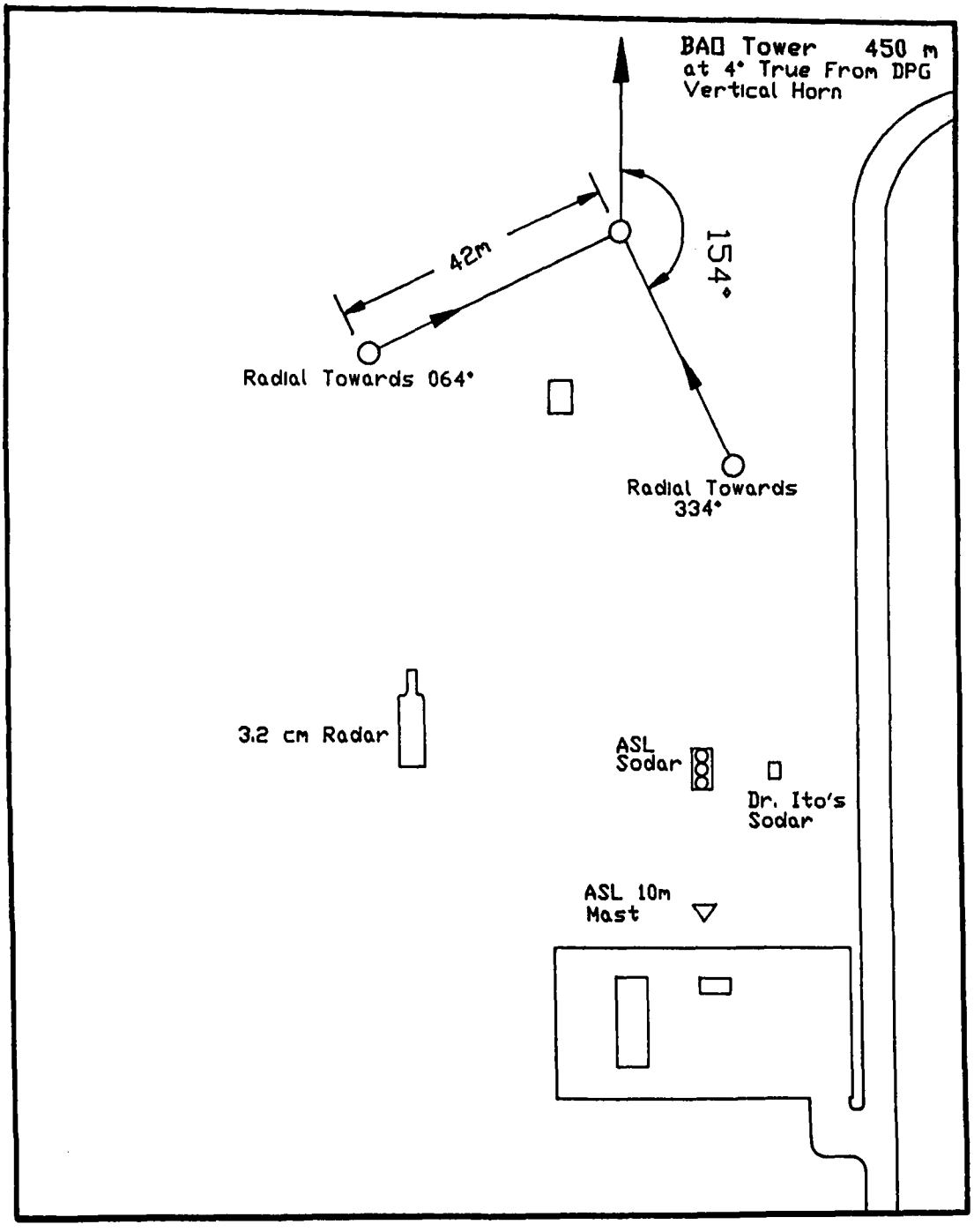

Figure 1. ISIE Experimental Configuration near the BAO Entrance Showing Detail of the DPG Sodar Configuration with the Three Horns Located at Positions Indicated by Circles. Arrows Toward the Vertical Horn Indicate Direction of Off-Axis Horn Alignment. Locations of the ASL Sodar, the Japanese Sodar, and the NOAA Radar are also Indicated.

Data collected during the ISIE included wind speed (U), wind direction (θ), wind direction standard deviation (σ_θ), and vertical wind standard deviation (σ_w). Additional detailed performance information, including data from the three radial wind components, was collected on the DPG sodar. The basic data averaging period was 20 min. The DPG sodar height range was limited to 250 m with a range resolution of 25 m, which allowed a relatively fast pulse repetition frequency (PRF) of 0.11 Hz for each horn. The other sodars were set for longer ranges and consequently had slower PRFs. Sodar 20-min averaged data were compared to 20-min averaged data obtained from the BAO tower. To date, analyses have been performed only on the computed wind and turbulence data. Consequently, the results must be considered preliminary.

Wind and turbulence data from the BAO tower were used for reference during the ISIE. The BAO tower was instrumented at 50-m intervals with three-axis sonic anemometers and propeller-vane anemometers. The sonic anemometers were mounted on booms facing towards the south-southeast, while the propeller-vane anemometers were mounted on the opposite side of the tower facing towards the north-northwest. When the wind directions had a southerly component, the sonic anemometers were free of the BAO tower shadow and were used for the intercomparisons. Otherwise, the propeller-vane data were used. The BAO tower and its instrumentation are described in detail by Kaimal and Gaynor (1983).

The initial data analysis consisted of intercomparisons of sodar 20-min averaged winds with the corresponding winds measured on the BAO tower, which was 450 m north of the DPG sodar's vertical horn. Plots of the DPG sodar versus the BAO tower wind speed and direction results for the 150 m level, provided by Dr. Bruce Baker, are presented in Figures 2 and 3.

The preliminary ISIE results were disappointing. The sodars demonstrated a capability to measure wind speed and direction averaged over a 20-min period, but only over a limited wind-speed range. The wind-speed measurements in Figure 2 show a trend towards underspeeding at speeds in excess of 8 m/s. This trend was present in data from all of the sodars and produced progressively less reliable data as wind speeds increased. The Remtech sodar data quality algorithms seldom validated data for wind speeds in excess of 14 m/s. The other sodars occasionally reported winds over 20 m/s, but with considerable underspeeding compared to the BAO tower winds. The DPG sodar results were somewhat worse than those for the other sodars. This is thought to be due to deficiencies in data reduction algorithms. A detailed investigation of these results will be performed when the complete ISIE data set becomes available.

Sodar operation becomes increasingly difficult in high wind speeds because higher winds increase the background noise level and induce mixing that decreases the effectiveness of the scattering medium. The wind also deforms the acoustic beam path so that the backscatter volume is no longer along the antenna axis. These effects decrease the number of valid echo returns available for averaging. Beam bending also alters travel time along the acoustic path, creating range uncertainties. A detailed analysis of the radial data is required to define the exact cause of the underspeeding tendency found in the ISIE.

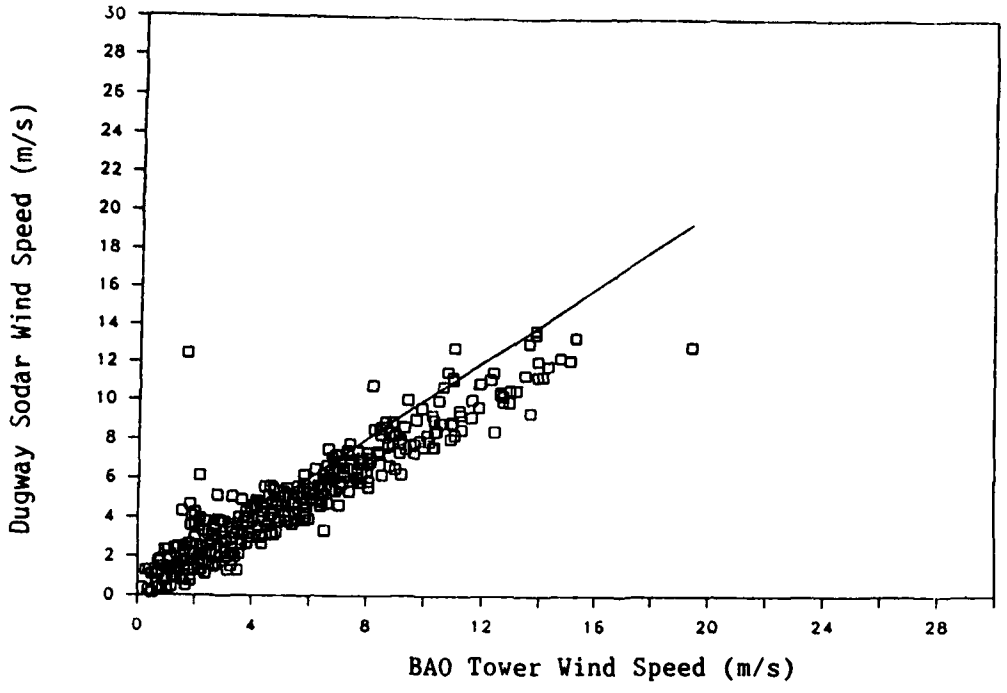

Figure 2. Plot of Wind Speeds Measured at 150 m by the DPG Sodar and the BAO Tower Data (Data Plots by Dr. Bruce Baker).

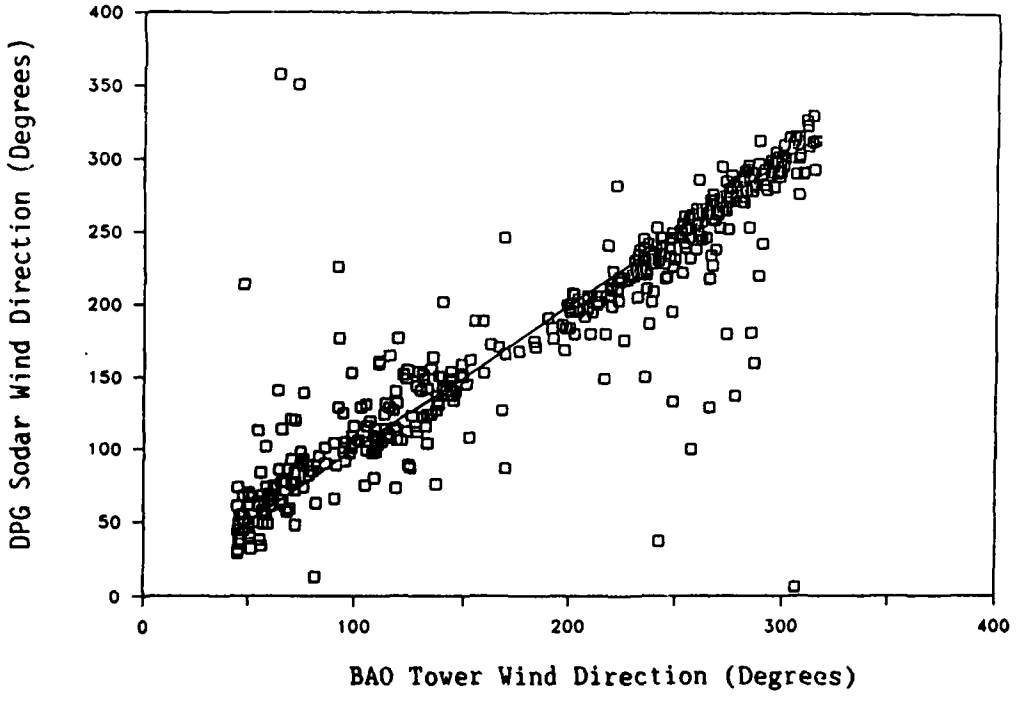

Figure 3. Plot of Wind Directions at Measured 150 m by the DPG Sodar and the BAO Tower Data (Data Plots by Dr. Bruce Baker).

The wind directions plotted in Figure 3 do not indicate any angle-dependent trends in the data. A majority of the data points lie within ±50 deg of the values measured at the BAO tower. Outlying data points are associated with very low or very high wind speeds and strong trends in wind direction. A more detailed analysis of sodar performance under these conditions will be provided when the complete ISIE data set becomes available.

A major objective of the ISIE was to test the turbulence measurement capabilities of sodars. The DPG sodar and BAO tower measurements of the standard deviations of the vertical wind velocity σ_w and horizontal wind direction σ_θ are compared in Figures 4 and 5, respectively. A significant trend towards underestimation of σ_w exists in the DPG sodar returns. This trend increases with increasing σ_w. The AV and REM sodar σ_w profiles have some scatter, but exhibit no comparable trend. The trend in the DPG sodar data σ_w may indicate a problem with the data processing algorithm. A future attempt to resolve this question will be made by analyzing the radial returns.

The σ_θ plot in Figure 5 shows widely scattered returns with very little relationship between the DPG sodar and BAO tower data. Similar σ_θ results were found for the other acoustic sounders, indicating that this is a systemic deficiency that is not peculiar to the DPG sodar. Acoustic sounder wind direction standard deviation is derived from the radial data using an assumption that horizontal and vertical motions are correlated (Remtech, 1985). Because the DPG sodar off-axis radials are oriented 15.5 deg off vertical, the data include contributions from both horizontal and vertical wind motions. When estimating the mean horizontal wind, the mean vertical wind velocity is usually a small term that can be subtracted from the radial data with a fair degree of accuracy. To obtain σ_θ, the σ_w obtained from the vertically oriented radial must be subtracted from the off-vertical radial data. Unfortunately, σ_w is not a small term, and the correlation between σ_θ and σ_w is an unknown that exhibits considerable variability. Assumptions that this correlation is either one or zero are likely to be seriously in error.

2.3 THE SCINTILLOMETER WEIGHTING FUNCTION TEST

Two prototype crosswind scintillometers were built for DPG by the NOAA ERL/WPL to obtain the simultaneous temporally and spatially-averaged wind measurements needed to define near-surface wind flow patterns for chemical simulant, smoke/obscurant, and other dissemination tests. The crosswind scintillometer consists of a transmitter and a downrange receiver aligned to define an optical path of length L. Crosswind measurements are obtained at five segments along the optical path, providing a unique remote wind measurement capability.

The crosswind scintillometer transmitter uses a 0.94-μm LED radiating over a 1.8-mm diameter hemisphere as a source, with a ground glass diffuser to enlarge its radiating area. Two 20- by 40- cm Fresnel lenses with alternating clear and reflecting stripes form zero-mean filters (d_t) of 20- and 5- cm wavelengths. Receiver optics consist of one 29- by 40- cm Fresnel lens forming three pairs of zero mean filters (d_r) of 5-, 10-, and 20-cm wavelengths. Ratios of the transmitter and receiver zero mean filter wavelengths define spatial filters of wavelength w at path position z as

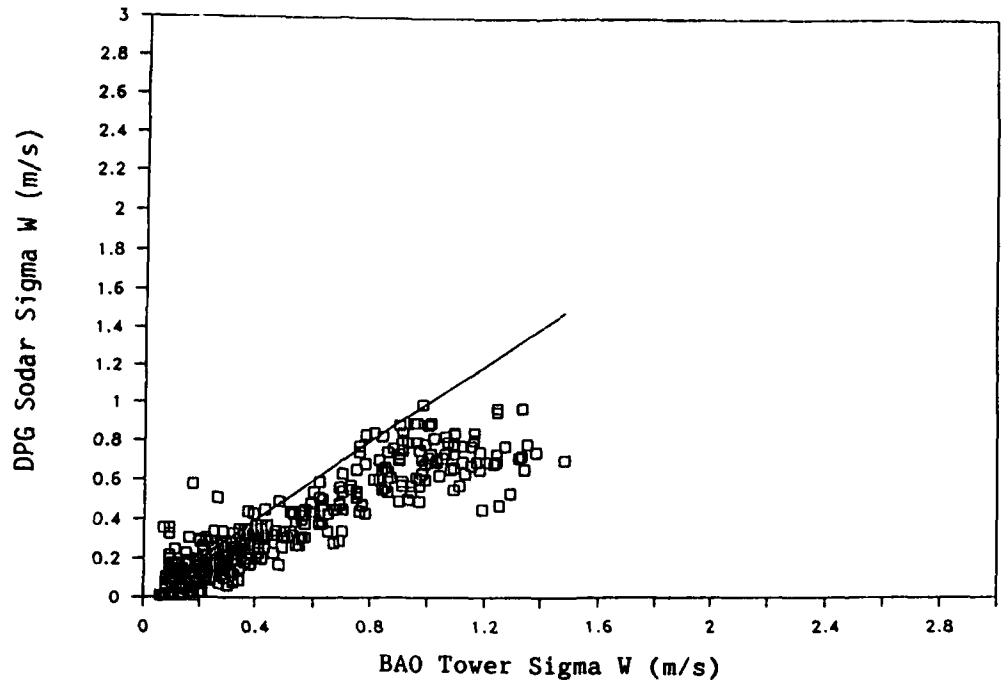

Figure 4. Comparisons of the Standard Deviations of the Vertical Wind Velocity Measured at 150 m by the DPG sodar and the BAO Tower Instruments, (Data Plots by Dr. Bruce Baker).

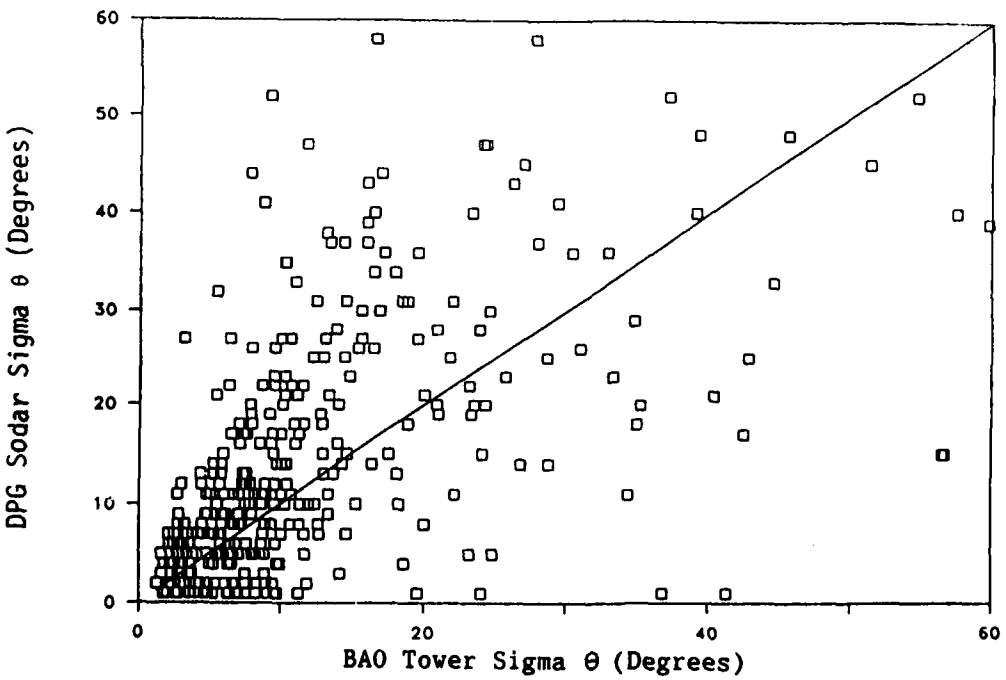

Figure 5. Comparisons of the Horizontal Wind Angle Standard Deviation Measured at 150 m by the DPG Sodar and the BAO Tower Instruments (Data Plots by Dr. Bruce Baker).

$$w = d_r d_t/(d_r + d_t) \quad (5)$$

$$z = L/(1 + d_r/d_t) \quad (6)$$

The spatial filters define the size of the turbulent eddies that contribute the strongest signals received from each path segment. The combinations of transmitter and receiver filters produce weighting functions at positions along the the optical path as shown in Figure 6. Fractional path position z is defined between zero (L = 0.0) at the transmitter and one (L = 1.0) at the receiver in Figure 6. The relationships between zero-mean filter element size, path position, and spatial wavelength are given in Table 3.

Scintillometer performance is highly dependent on the path weighting functions shown in Figure 6. The Scintillometer Weighting Function Test was designed to verify these weighting functions by intercomparing crosswind scintillometer winds with wind measurements made by sonic anemometers stationed at each weighting function peak along the optical path. Scintillometer weighting functions are difficult to verify in the atmosphere because wind components along the path are correlated to varying degrees over the range of atmospheric motion scales. These correlations are unknowns that are continuosuly changing in response to the atmosphere's dynamical forcing functions. One way to check the weighting functions is to impose a perturbation on the wind field that moves from one path segment to another. The decorrelation effects of this perturbation should permit evaluation of the weighting functions. This moving perturbation was achieved by flying a UH-1 helicopter slowly at low elevations along a path parallel to the crosswind scintillometer's optical path.

The Scintillometer Weighting Function Test was conducted on 7 March 1989 with an 800-m optical path established between the DPG Tower Grid Command Post and Mesonet Station 1. Five sonic anemometers were placed on a line adjacent to the optical path at locations corresponding to the locations where the weighting function peaks should occur. Analog data from all instruments were logged at a 1-Hz rate on CA-21 data loggers. The UH-1 rotor wash knocked over the sonic anemometer positioned near the 1/3 path segment, but all other instrument positions remained intact. Data from these trials are awaiting reduction and analysis, and a report on the results will be included in the Part II report.

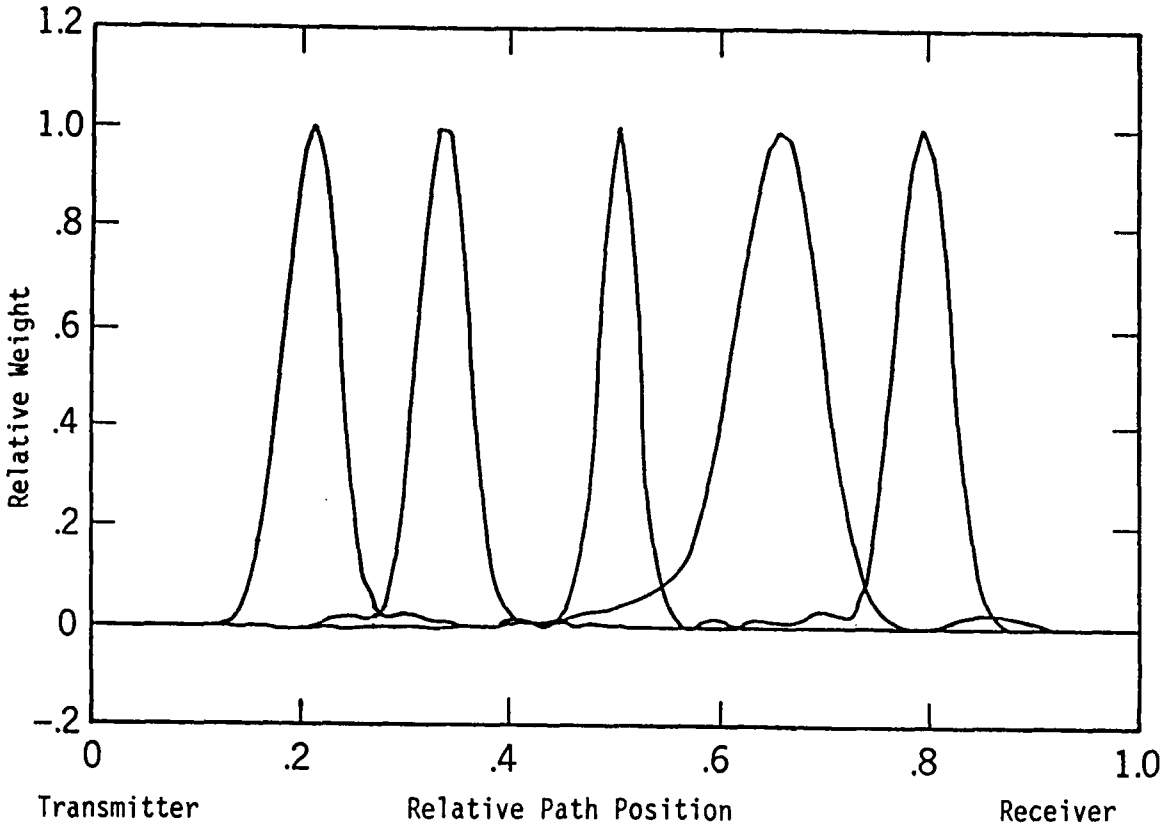

Figure 6. Calculated Path Weighting Functions (Courtesy of Gerard Ochs, NOAA ERL/WPL).

Table 3. Relationship Between Transmitter/Receiver Filter Element Size, Path Position, and Spatial Wavelength.

Zero-Mean Filter			
Transmitter d_t (cm)	Receiver d_r (cm)	Path Position z/L	Spatial Wavelength w (cm)
5	20	1/5	4.00
5	10	1/3	3.33
5	5	1/2	2.50
20	10	2/3	6.67
20	5	4/5	4.00

SECTION 3. APPENDICES

APPENDIX A.
METHODOLOGY INVESTIGATION PROPOSAL AND DIRECTIVE

RDT&E Methodology Proposal - FY89

1. TITLE. Calibration and QC for New Meteorological Instrumentation, Part I.

2. INSTALLATION/FIELD OPERATING ACTIVITY. U.S. Army Dugway Proving Ground, Dugway, UT 84022-5000.

3. PRINCIPAL INVESTIGATOR. Mr. Christopher A. Biltoft
Meteorology Division
STEDP-MT-M
Autovon 789-5101
GROSS@DPG-MT.ARPA

4. BACKGROUND. DPG has acquired or is in the process of acquiring new meteorological instrumentation such as Doppler acoustic sounders and a continuous atmospheric wind profiler. DPG is also acquiring digital data systems to handle the large volumes of data from the new instrumentation.

5. PROBLEM. To make full use of its new meteorological instrumentation, DPG needs to develop calibration and QC procedures for the new instrumentation and adapt the new data to DPG's specific needs.

6. OBJECTIVE. Develop calibration and QC procedures for DPG's new meteorological instrumentation and tailor the data available from the new instrumentation to meet DPG meteorological test support requirements.

7. MISSION AREAS SUPPORTED. All field tests conducted at DPG will benefit, including mission areas such as combat support (NBC detection/warning, smoke/obscurants, etc.) and fire support (MLRS, etc.).

8. PROCEDURES.

a. Develop scintillometer data reduction and QC procedures for use with the new digital data acquisition system (November 1988).

b. Develop software to transfer data from the new digital data acquisition system to the displays in the new Mission Control Center (MCC) (April 1989).

c. Develop software for real-time display and QC of meteorological data in the new MCC (June 1989).

d. Develop software to integrate the continuous atmospheric profiler into DPG data archival and display system (July 1989).

e. Complete Doppler acoustic sounder (sodar) QC procedures based on analyses of results of the International Sodar Intercomparison experiment. Sodar calibration and QC procedures will be coordinated with appropriate American Society for Testing of Materials (ASTM) and Range Commander's Council (RCC) working groups (September 1989).

9. JUSTIFICATION/IMPACT. Field tests at DPG are documented by detailed meteorological measurements to enable assessments of meteorological influences

on test results. Data from current field tests are often compared with data from previous test series to identify differences in munition performance or effectiveness. Meaningful analyses and comparisons of meteorological influences on test results require that the accuracy of the meteorological measurements be established and documented. Failure to develop calibration and QC procedures for DPG's new meteorological instrumentation will limit the value of test data sets and/or restrict the use of the new instrumentation. If this investigation is not funded, the rate of return on DPG's investment in new meteorological instrumentation will be considerably reduced.

10. DOLLAR SAVINGS. NA.

11. RESOURCES.

a. Financial.

	Dollars (Thousands) FY89	
	In-House	Out-of-House
Personnel Compensation	17.5	0.0
Travel	2.0	0.0
Materials and Supplies	0.5	0.0
Subtotals	20.0	0.0
FY Total	20.0	

b. Explanation of Cost Categories.

(1) Personnel Compensation. Compensation for federal civilian employees assigned to the methodology investigation.

(2) Travel. To coordinate and consult with personnel working on similar problems (two trips).

c. Obligation Plan.

FQ	1	2	3	4	TOTAL
Obligation Rate (Thousands)	5.0	5.0	5.0	5.0	20.0

d. Man-Hours Required. Approximately 795 in-house direct labor hours and no contract labor hours will be required to complete this investigaiton.

12. ASSOCIATION WITH TOP PROGRAM.

a. No TOPs will be revised as a result of this investigation.

b. No new TOPs are contemplated. However, it is anticipated that calibration and QC procedures will be established for DPG Doppler acoustic sounders.

13. AUTHENTICATION.

DEPARTMENT OF THE ARMY
HEADQUARTERS, U.S. ARMY TEST AND EVALUATION COMMAND
ABERDEEN PROVING GROUND, MARYLAND 21005-5055

REPLY TO ATTENTION OF

MT-A

26 SEP 1988

AMSTE-TC-M (70-10p)

MEMORANDUM FOR: Commander, U.S. Army Dugway Proving Ground, ATTN: STEDP-MT-A, Dugway, UT 84022-5202

SUBJECT: FY 89 RDTE Methodology Improvement Program Grant

1. This memorandum advises that grants have been made for the investigations listed in enclosure 1 under the TECOM Methodology Improvement Program 1W665702D628.

2. The MIPs submitted in the FY 89-95 SOLID MIND are the basis for headquarters approval of the investigations.

3. Special instructions:

a. Although it is expected that literature searches were conducted prior to submitting a methodology investigation proposal (MIP) to ensure that the MIP did not duplicate work already performed, further searches should be made prior to investigation initiation to ensure that recent work performed by others will not change or obviate the need for the investigation about to begin.

b. All reporting, including final technical reports prepared by contractors, will be in consonance with paragraph 2-6 of the reference. The final report will be submitted to this headquarters, ATTN: AMSTE-TC-M, in consonance with Test Event 570/580. Each project shall be completed in FY 89 as reflected in the scheduling.

c. Recommendations for new TOPs or revisions to existing TOPs will be included as part of the recommendation section of the final technical report. Final decision on the scope of the TOP effort will be made by this headquarters as part of the final technical report approval process.

d. The addressee will determine whether any classified information is involved, and will assure that proper security measures are taken when appropriate. All OPSEC guidance will be followed strictly during each investigation.

e. Prior to investigation execution, the test activity will verify that no safety or potential health hazards to humans participating in testing exist. If safety or health hazards do exist, the test activity will provide a safety/health hazards assessment statement to this headquarters prior to investigation initiation.

AMSTE-TC-M
SUBJECT: FY 89 RDTE Methodology Improvement Program Grant

f. Environmental documentation for support tests or special studies is the responsibility of the test activity and will be accomplished prior to initiation of the investigation.

g. Upon receipt of this grant notification, test milestone schedules as established in TRMS II data base will be reviewed in light of other known work load and projected available resources. If rescheduling is necessary and the sponsor nonconcurs, a letter citing particulars, together with recommendations, will be forwarded to Commander, U.S. Army Test and Evaluation Command, ATTN: AMSTE-TC-M, with an information copy to AMSTE-TA-O, no later than 15 calendar days from the date of this memorandum. Reschedules concurred in by the sponsor can be entered directly along with a properly coded narrative by your installation/test activity.

h. All work shall be performed such that energy conservation is considered throughout the effort.

i. FY 89 RDTE funds authorized for the investigations are listed on enclosure 1. GOA Form 1006 will be forwarded by the TECOM Resource Management Directorate. A cost estimate shall be submitted within 30 days following receipt of this grant notification.

4. Reference Draft TECOM Regulation 70-12, dated 27 June 1988, TECOM Methodology Improvement and Standardization Programs.

5. Point of contact, this headquarters, is Mr. James Piro, AMSTE-TC-M, amstetcm@apg-4.apg.army.mil, AUTOVON 298-2170/3677.

FOR THE COMMANDER:

Grover H. Shelton

Encl

GROVER H. SHELTON
Chief, Meth Imprv Div
Directorate for Technology

APPENDIX B. LIGHT TUNNEL ANEMOMETER STUDIES

B.1. INTRODUCTION

When instruments based on fundamentally different principles are used to measure a common variable, discrepancies in the results inevitably lead to questions concerning instrument performance. This applies to the measurement of wind speed using cup and sonic anemometers. Cup anemometer wind speed is determined from rotor assembly rotation rate, while sonic anemometer wind speed is determined from the transit time of acoustic pulses. The major discrepancies between cup and sonic anemometer wind measurements are attributed to data processing (DP) differences and to differences in performance when exposed to turbulent flow. Turbulence effects are of particular concern because anemometer calibrations are performed in low turbulence wind tunnels, whereas wind measurements are generally made in the fully turbulent atmosphere.

In an effort to better understand the differences in cup versus sonic anemometer performance under turbulent conditions, a set of trials was conducted on 28 February 1989 at the DPG Light Tunnel facility using co-located cup and sonic anemometers. Trial data evaluation included the removal of DP differences and the analysis of turbulence scale and intensity effects on anemometer performance.

B.2. INSTRUMENTATION

The anemometers used in the Light Tunnel tests were one 2-axis Applied Technologies, Inc. (ATI) sonic anemometer (RSWS-201/28, #870603) with a coplanar orthogonal transducer array of 15-cm pathlength, and two research-grade Climet 011-1 transmitters (serial number 155 and 176) with Climet 014-5 rotor assemblies. Analog data from all instruments were logged on Campbell Scientific CA21 data loggers at a 10-Hz rate. The Light Tunnel has dimensions of 3.5 m by 3.5 m and is 20 m in length. A large floor fan (61-cm diameter) rotating at 1800 revolutions per minute (rpm) was used to generate a controlled turbulent flow. The instruments were mounted 3.6 m downstream of the fan at a height of 1.8 m above the floor.

B.2.1. The Sonic Anemometer. The sonic anemometer consists of paired sets of acoustic transmitters and receivers, with microprocessor circuitry to count intervals of time between transmission and reception of sound pulses. The fundamental measurement unit is transit time which, with a known transit distance or pathlength, is converted to velocity. Sonic anemometer performance is a function of clock time resolution, precision of the acoustic pathlength determination, and an algorithm that compensates for flow distortion due to wake effects from the sonic anemometer transducer array. Sonic anemometer output is a series of velocity readings averaged to 10 Hz. Velocity components measured along the transducer array are converted to wind speeds by calculating the square root of the sum of the squares of velocity components, as described in Section 3. Alongwind and crosswind means, variances, and covariances are derived using software routines.

Inverse transit time solutions are used in the ATI sonic anemometer. Subtraction of the inverse transit times eliminates speed of sound from the basic sonic anemometer equation, giving the velocity component v_s along each axis as

$$v_s = \frac{d}{2}\left[\frac{1}{t_1} - \frac{1}{t_2}\right] \qquad \text{(B-1)}$$

where t_1 and t_2 are transit times of acoustic pulses traveling in opposite directions between a transducer pair and d is the acoustic pathlength between transducers. ATI states that the velocity component measurement uncertainty is 0.05 m/s. Velocity components from two horizontal orthogonal axes can be converted into the wind speed and direction.

Sonic anemometers are well suited for micrometeorological turbulence measurements in the atmospheric boundary layer because they have virtually inertia-free, quasi-instantaneous response to turbulent variations in the winds. The spatial resolution of the instrument is determined by its pathlength. Silverman (1968) found that spatial averaging effects become noticeable at turbulence wavelengths shorter than 2π times the instrument's spatial resolution. Consequently, spatial resolution losses are expected for turbulence scales smaller than 1 m, with progressively increasing losses at smaller turbulence scales.

Sonic anemometers suffer transducer shadowing effects when the acoustic path and downwind transducer lie within the wake of the upwind transducer and/or its supporting structure. Accordingly, Kaimal (1979) suggested an algorithm to compensate for wake effects on velocity component measurements. The algorithm, which adjusts for a linear drop in the measured velocity component v_{sm} when the angle of the wind to the transducer axis is less than 75°, is

$$v_s = \begin{cases} \dfrac{V_{sm}}{A+B|\theta|/75}, & 0° \leq |\theta| \leq 75° \\ V_{sm}, & 75° < |\theta| \leq 90° \end{cases} \qquad \text{(B-2)}$$

where A and B are constants dependent on the acoustic pathlength and $|\theta|$ is the absolute value of the apparent wind angle with respect to the transducer axis. For this sonic anemometer, constant A is 0.824 and B is 0.176. A version of this algorithm was installed in the sonic anemometer software used in the Light Tunnel tests.

Depending on how the data are averaged, the sonic anemometer velocity component measurements can be used to calculate a mean scalar wind speed or a mean vector velocity. The scalar speed is the square root of the sum of the squares of the individual along-axis (u_{si}) and cross-axis (v_{si}) velocity components, the resultant being divided by sample size n

$$WS_{(scalar)} = \frac{1}{n}\left(\sum_{i=1}^{n} [u_{si}^2 + v_{si}^2]^{1/2}\right) \qquad \text{(B-3)}$$

The mean vector velocity is the square root of the sum of the squares of the mean along-axis (u_s) and cross-axis (v_s) velocity components

$$WS_{(vector)} = [\bar{u}_s^{\,2} + \bar{v}_s^{\,2}]^{1/2} \tag{B-4}$$

where $\bar{u}_s$ and $\bar{v}_s$ are defined by

$$\bar{u}_s = \frac{1}{n}\left(\sum_{i=1}^{n} u_{si}\right) \tag{B-5}$$

$$\bar{v}_s = \frac{1}{n}\left(\sum_{i=1}^{n} v_{si}\right) \tag{B-6}$$

The effects of turbulence scale and intensity on the sonic anemometer performance are not quantitatively known. Qualitatively, turbulence of a scale comparable to the wake scale should broaden the wake, diminish the wake velocity deficit, and create a more uniform velocity deficit distribution across the wake. Velocity deficits due to wake effects have been measured in wind tunnel studies by Baker et al. (1989). The Baker et al. study also identifies a velocity dependence in the wake effects compensation algorithm [Equation B-2] that creates an absolute measurement uncertainty on the order of 3 to 5 percent. These results have not been verified under fully turbulent conditions, but the measurement uncertainty should be somewhat less under these conditions. Intercomparison tests conducted under fully turbulent conditions (Hanafusa et al., 1982, unpublished tests at the Boulder Atmospheric Observatory) have failed to identify uncompensated deficits in velocity or turbulence measurements due to wake effects. This disparity with wind tunnel findings may be due in part to the absence of an absolute reference for the intercomparison tests conducted outside the wind tunnel.

B.2.2 The Cup Anemometer. The Climet cup anemometer consists of a 3-cup rotor assembly mounted on a rotating shaft that rests on low friction bearings within the transmitter. The shaft assembly rotates as a consequence of the assymmetrical cup shapes that cause a larger drag coefficient for the cup's concave side than for the cup's convex side. As wind flows past the assembly, the assymmetrical drag causes an imbalance of forces that generates a torque T on the rotor. The assembly rotates at speeds above breakaway threshold where the aerodynamic torque provided by the wind's interaction with the cups overcomes the frictional torque of the bearings. Above threshold, the rotor assembly responds to wind speed variations by increasing or decreasing rotation speed until forces balance. A precision light beam chopper within the rotor assembly produces pulse counts proportional to rotation speed Ω. Pulse counts that define Ω are converted to analog voltages by a translator.

When the forces applied to a cup anemometer balance, the net torque is zero and the mean wind speed $\bar{u}$ is obtained from a transfer function

$$\bar{u} = C + \Omega/D \qquad \text{(B-7)}$$

where $\bar{u}$ is the wind speed and Ω is the frequency in revolutions per second. Coefficient C is a zero offset and coefficient D describes the ratio of rotor angular velocity to wind speed. For the Climet 011-1 transmitter with a 014-5 rotor assembly, the magnitudes of C and D were determined to be 0.52 and 0.3187, respectively, when $\bar{u}$ is in miles per hour (Climet Instruments Inc., 1964). These coefficients were determined in a wind tunnel calibration performed at the National Bureau of Standards, Washington, DC (File Nr. 6.3/179988). Equation (B-7) is valid for $\bar{u}$ above u_1, where u_1 is the lower end of the rotor's linear response. At lower speeds, the frictional torque causes a deviation from Equation (B-7).

A cup anemometer's performance is usually specified by its breakaway or threshold wind speed u_1 and distance constant λ. The distance constant is defined (Lockhart, 1987) as "the distance the air flows past a rotating anemometer during the time it takes the cup wheel or propeller to reach (1-1/e) or 63% of the equilibrium speed after a step change in wind speed". For steady wind conditions, λ is nearly constant over the anemometer's operating range. The Climet Model 011-1 table of specifications gives the threshold as 0.6 mph and the distance constant as less than 5 ft. The distance constant is related to a response time τ by

$$\lambda = \tau\bar{u} \qquad \text{(B-8)}$$

Thus, τ varies inversely with $\bar{u}$. Because λ cannot be measured directly, it is usually obtained from wind tunnel tests with u held constant and τ determined by monitoring anemometer response as the rotor assembly is released from a restrained condition.

The distance constants for the cup anemometer rotor assembly and the cup anemometer measurement system can differ because chopper-based anemometer systems contain filters used to smooth the pulse train. A low-pass resistance capacitive (RC) filter is used in the Dugway version of the Climet translators to minimize pulse train ripple. Snow et al. (1989) demonstrated that a cup anemometer system consisting of a rotor assembly and electronic circuitry behaves as an overdamped second-order system, the dynamic performance of which is characterized by response times for the rotor assembly (τ_r) and the filter circuit (τ_c). Estimates of τ_r and τ_c obtained using Climet cup anemometer performance curves indicate that $\tau_r > \tau_c$ for wind speeds on the order of 2 m/s. Therefore, system response was dominated by the rotor and its time constant for the wind velocity of about 2 m/s used in the Light Tunnel trials.

Following MacCready and Jex (1964), the response of a cup anemometer rotor assembly rotating at angular velocity Ω is modeled by the first-order linear differential equation

$$\tau \left(\frac{d\Omega}{dt}\right) + \Omega = f(t) \qquad \text{(B-9)}$$

where f(t) is a forcing function representing external input from the velocity field, and τ equals τ_r. With f(t) set to zero, the transient solution for Equation (B-9) is

$$\Omega = e^{-(t-t_1)/\tau} \tag{B-10}$$

where t_1 is a lag time between the arrival of an impulse at the rotor assembly and the moment when the rotor begins to respond with first-order behavior. A useful discussion of lag time is found in Snow et al. (1989). For the low velocities used in the Light Tunnel studies, it can be safely assumed that $t_1 << \tau$. Using Equations (B-7) and (B-10) with a step change in speed from u to $u_f > u_1$ at time t equal to 0, the solution for Equation (B-9) is

$$\Omega(t) = \begin{cases} D\ (\bar{u}_i - C) & , 0 \leq t \leq t_1 \\ D\ (\bar{u} - C) + [D\ (u_f - \bar{u})]\ (1 - e^{-(t-t_1)/\tau}) & , t > t_1 \end{cases} \tag{B-11}$$

First-order solutions such as Equation (B-11) provide only a rough approximation of cup anemometer response. Departures from first-order response in the form of cup overspeeding become significant for applications in turbulent flow. The most apparent departure from first-order response occurs because τ varies inversely with wind speed. Consequently, τ decreases during accelerating flow and increases during decelerating flow. The resultant overspeeding has been recognized since Sabinin's analysis of the problem in 1923 (see Kaganov and Yaglom, 1976). The variable τ effect is compounded by a cup anemometer's inertia and asymmetry. Inequalities in the drag coefficient for the cup's concave versus convex sides cause a more rapid gain in kinetic energy during spin up than the corresponding loss of kinetic energy during spin down. The result, described by Hayashi (1987) and Lockhart (1987), is that a distance constant determined during spin up (λ_a) is smaller than a distance constant determined during spin down (λ_d). Other sources of uncertainty include off-axis response due to interaction with the vertical wind component (MacCready, 1966) and small nonlinearities in response (Hyson, 1972). These effects are additive and increase with increasing turbulence intensity. None of these effects are addressed during the usual cup anemometer calibrations in low turbulence wind tunnels.

The complexity of cup anemometer response in turbulence has prevented the development of an explicit general solution for overspeeding. The best efforts to date have produced analytic approximations for specific anemometers operated within a limited range of turbulence intensity. A general analytic expression for overspeeding must include both turbulence intensity and turbulence scale effects. The overspeed ratio $(u_{cup}-u)/u$ is the product of these effects, integrated over the applicable range of turbulent wavelengths (Λ) or wavenumbers (κ):

$$(\bar{u}_{cup}-\bar{u})/\bar{u} = \frac{\int_0^\infty \{\text{Intensity Effects}\}\ \{\text{Scale Effects}\}d\kappa}{\int_0^\infty d\kappa} \qquad \text{(B-12)}$$

Turbulence intensity effects include both on-axis (horizontal) and off-axis (vertical) turbulence components. Expressions derived by Wyngaard et al. (1974) describe horizontal wind component turbulence effects as a function of the square of the turbulence intensity. If rotor assembly response is symmetric about its vertical axis (i.e., independent of the sign of the angle of attack) and if the mean vertical velocity is essentially zero, the off-axis contribution to overspeeding is also proportional to the square of the vertical component of turbulence intensity. Off-axis response asymmetry is usually attributed to the transmitter housing and other structural features that become obstacles to flow. For the DPG cup anemometer, the effect of these features is negligible at angles of attack normally encountered in ambient flow. Therefore, intensity effects can be expressed as the velocity variance contributions divided by the square of the mean wind speed. That is,

$$\{\text{Intensity Effects}\} = \left\{\frac{E}{\bar{u}^2}\left[\sigma_u^2(\kappa) + \sigma_v^2(\kappa)\right] + \frac{F}{\bar{u}^2}\left[\sigma_w^2(\kappa)\right]\right\} \qquad \text{(B-13)}$$

where σ_u^2 and σ_v^2 represent the alongwind and crosswind velocity variances and σ_w^2 represents the vertical velocity variance. Coefficients E and F are empirically determined, anemometer-specific constants with magnitudes near 1.0.

Turbulence scale effects include variation of the overspeed response and amplitude gain as functions of wavelength. The overspeed response reaches a maximum for wavelengths shorter than the anemometer's distance constant and decreases with increasing wavelengths as the rotor assembly is able to adjust more completely to changes in speed. Conversely, amplitude gain increases at longer wavelengths. The net turbulence scale effect is the product of the overspeed response and amplitude gain. This net effect causes greater overspeeding for turbulence scales near the cup anemometer's distance constant than for scales that are much larger or smaller than the distance constant.

Turbulence scale effects are conveniently represented by normalizing turbulent wavelength Λ by the anemometer's average distance constant λ_n, where

$$\lambda_n = (\lambda_a + \lambda_d)/2 \qquad \text{(B-14)}$$

The normalized, dimensionless wavelength Λ^* is

$$\Lambda^* = \Lambda/\lambda_n = 1/\kappa^* \qquad \text{(B-15)}$$

where K^* is the normalized, dimensionless wavenumber. Turbulence scale effects are modeled by expressions that include the product of the amplitude and response effects. These effects are approximated by exponential functions of the normalized wavenumber. That is,

$$\{\text{Scale Effects}\} = \{[\text{Response Effect}][\text{Amplitude Effect}]\} = \{[e^{-G/K^*}][e^{-HK^*}]\} \quad \text{(B-16)}$$

where G and H are empirical coefficients with magnitudes near 0.1 and 0.8, respectively. Figures 4 and 5 of Hayashi (1987) and the λ_n for the anemometer routinely used by the Japanese Meteorological Agency were used to obtain these estimates of G and H. The coefficients G and H may vary slightly for different anemometers, but the overall scale effects are likely to be similar for modern cup anemometer designs. The product of the two exponential terms in Equation (B-16) is a scale effects multiplier for each Λ^*, as illustrated in Figure B-1. Virtually all of the turbulence scale effects are contained within a band bounded by 0.2 and 40 Λ^*, with the maximum effect between 0.7 and 12 Λ^*.

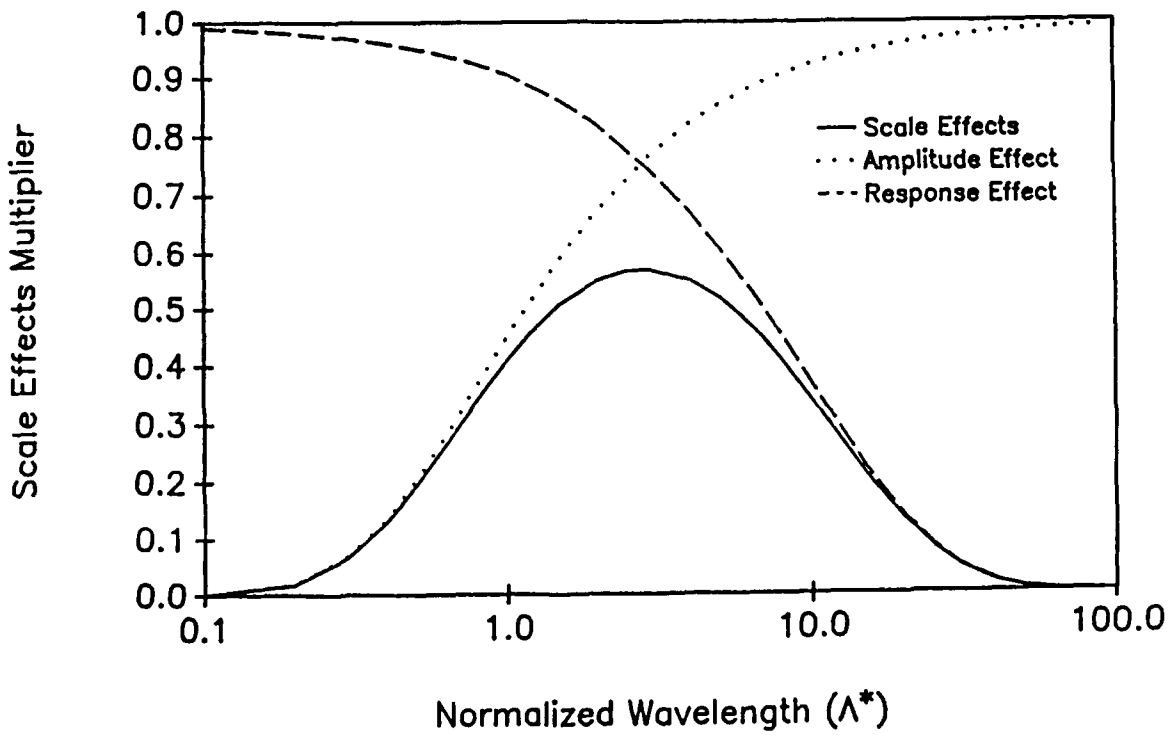

Figure B-1. Illustration of the Equation (B-16) Response Effect (dashed curve), Amplitude Effect (dotted curve), and the Combined Scale Effect (Solid Curve) as Functions of Normalized Wavelength Λ^*.

Combining Equations (B-12) through (B-16), a general equation for the effects of turbulence scale and intensity effects on cup anemometer overspeeding, integrated over all applicable wavenumbers, is

$$(\bar{u}_{cup}-\bar{u})/\bar{u} = \int_0^\infty \frac{E}{\bar{u}^2} \frac{[\sigma_u^2(\kappa^*) + \sigma_v^2(\kappa^*)][e^{-G/\kappa^*}][e^{-H\kappa^*}]d\kappa^*}{\int_0^\infty d\kappa^*} \qquad \text{(B-17)}$$

$$+ \int_0^\infty \frac{F}{\bar{u}^2} \frac{[\sigma_w^2(\kappa^*)][e^{-J\kappa^*}]d\kappa^*}{\int_0^\infty d\kappa}$$

The horizontal turbulence intensity component in Equation (B-17) is modified by the product of both amplitude and overspeed effects, while the vertical turbulence intensity component is modified by another exponential with a constant J. The vertical component overspeed effect is due to the non-cosine response of a cup anemometer (MacCready, 1966), and cup design will influence the magnitudes of constants F and J. Because a cup anemometer responds to all scales of off-axis motions except scales much smaller than the distance constant, the off-axis overspeed function is likely to be similar to the amplitude effect function. The constant J is probably similar in magnitude to H, but there are no data currently available to test this hypothesis. Also, the constants G, H, and J, which are empirically determined by separately considering turbulence intensity and scale effects as the sole cause of overspeeding, probably change somewhat when the combined effects are considered as in Equation (B-17).

B.3. TIME SERIES ANALYSIS OF THE LIGHT TUNNEL TRIALS

The sonic anemometer with its sensor array inverted was mounted as close as possible to two Climet cup assemblies without causing detectable interference. The cup anemometers were positioned so that the concave sides passed below the sonic anemometer transducers, as shown in Figure B-2.

Light Tunnel data were collected over two 24-min periods. Trial 1 was conducted with the sonic anemometer array oriented at a 45° angle to the mean flow, and Trial 2 was conducted with the array u-axis oriented into the flow. Table B-1 gives trial-averaged scalar speeds measured by the cup and sonic anemometers, and the vector velocity for the sonic anemometer. Non-dimensional turbulence intensity, defined as the square root of the velocity variance divided by scalar mean speed, is also provided for the alongwind ($\sigma_u/\bar{u}=I_x$) and crosswind ($\sigma_v/\bar{u}=I_y$) sonic anemometer components. Turbulence intensities for the omni-directional cup anemometers are provided under the I_x heading.

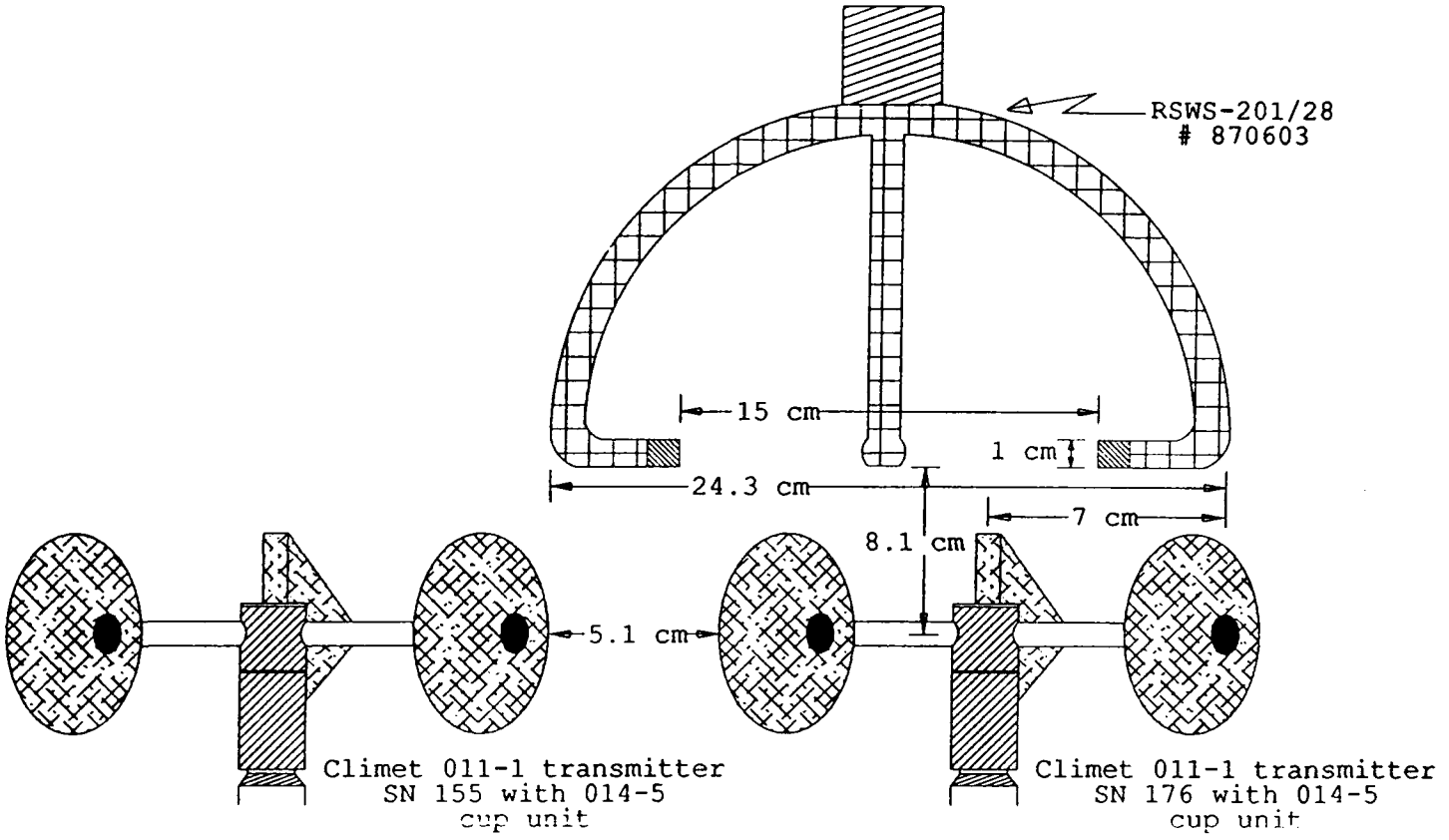

Figure B-2. Positions of the Climet Cup Units and ATI Sonic Anemometer Array for the Light Tunnel Study.

Table B-1. Summary of 28 February 1989 Light tunnel Trial Data.

Trial	Start Time (MST)	Instrument	Scalar Speed (m/s)	Vector Velocity (m/s)	Alongwind Turbulence Intensity I_x	Crosswind Turbulence Intensity I_y
1	0830	Sonic @ 45°	1.80	1.61	0.58	0.31
		Cup #155	2.03	--	0.32	--
		Cup #176	1.89	--	0.32	--
2	0906	Sonic @ 0°	1.80	1.63	0.59	0.31
		Cup #155	2.02	--	0.32	--
		Cup #176	1.83	--	0.31	--

Differences between the sonic anemometer scalar and vector mean winds on the order of 10 percent were obtained from data processed using Equations (B-3) and (B-4). This is the "DP difference", also known as the "DP-error" (MacCready, 1966). This difference should not be considered an error because, as pointed out by Lockhart (1987), it is solely the consequence of the data processing techniques used. Each DP technique has its own appropriate applications. The scalar DP technique provides wind speeds more comparable to those obtained from the cup anemometers.

The Light Tunnel trials provided the opportunity to test the performance of the sonic anemometer transducer shadow correction algorithm by comparing results from a sonic anemometer array oriented at 45 deg to the flow (Trial 1) with those from an array oriented directly into the flow (Trial 2). The actual array axes were oriented to within 2 deg of these nominal values. Although measurement differences induced by faults in the shadow correction algorithm should be maximized by comparing results for these two orientations, the sonic anemometer means and variances for Trials 1 and 2 are very similar. Any uncompensated differences due to transducer shadowing effects probably were masked by minor inter-trial variations in fan output. The absence of significant orientation-dependent velocity measurement differences indicates that the flow distortion correction algorithm installed in the sonic anemometer software (see Kaimal, 1979) does a reasonably good job of removing orientation angle dependencies from sonic anemoeter data.

Speed differences of 10 percent between Cup #155 and Cup #176 were observed in the Light Tunnel trials. Nearly identical results were achieved when transducer positions were exchanged. Consequently, the speed differences are considered to be an artifact of the non-uniform velocity field generated by the fan and not due to differences in cup performance.

The Light Tunnel trials provided an opportunity to compare the fluctuating signal responses of sonic and cup anemometers to turbulent flow. Figure (B-3) shows a 1-min segment of cup anemometer speed and sonic anemometer u-component (alongwind velocity component) fluctuating signal components with mean wind removed. The sonic anemometer response is virtually inertia free, whereas the

mechanical cup anemometer response requires a gain or loss of energy to achieve equilibrium with the turbulent flow. The sonic anemometer also has finer spatial resolution. Consequently, the sonic anemometer output is considered to be the "reference" in the comparison of response to turbulent flow.

The most apparent differences between cup and sonic anemometer response are the smoothing and phase lag exhibited by the cup anemometer. The smoothing effects, also known as dynamic gain or amplitude ratio, and phase lag are a consequence of the combined effects of rotor and electronic filter response times. These effects were modeled by MacCready and Jex (1964), and are illustrated for a range of sinusoidal frequencies in Figure 3 of Hayashi (1987). Response time effects on real wind data are also illustrated on Figure 10 of Kondo et al. (1971).

The effects of a variable time constant τ are evident from the slopes of the cup anemometer trace in Figure B-3. These slopes are systematically steeper during velocity increases than during velocity decreases. This is evidence of the rotor assembly spinning up in increasing wind speeds more rapidly than it spins down in response to decreasing wind speeds. This effect was confirmed by the Hayashi (1987) rotor spin up and spin down tests, which also led him to conclude that λ_a is less than λ_d.

B.4. AN ANALYSIS OF CUP ANEMOMETER OVERSPEEDING

Light tunnel turbulence intensity data were used with an approximation of Equation (B-17) to estimate Climet cup anemometer overspeeding. This process began with a review of the spectrum of the turbulent flow created by the fan, which differs in several respects from ambient atmospheric spectra. The fan-generated velocity spectrum contains rapidly evolving turbulence elements of higher intensity than usually encountered in the atmosphere, and does not exhibit the inertial subrange slope expected for ambient conditions. The bulk of the spectral energy is contained in a band ranging from 0.01 to 2.0 Hz, with a maximum near 0.024 Hz. For a mean flow speed of 1.8 m/s, the wavelength of this spectral maximum is 75 m. Because the fan-generated flow contains considerable turbulence in the scales that cause overspeeding in cup anemometers, it is therefore useful for the study of overspeeding effects.

The 10-Hz Light Tunnel trial data were used to generate spectrum summaries for both the cup and sonic anemometers. These spectra were subject to logarithmic averaging and tapering as described by Kaimal and Gaynor (1983). Ratios of the variances were then formed by dividing the cup anemometer variance by the corresponding sonic anemometer variance at each frequency interval. These normalized spectral responses, averaged for both trials, are presented as a function of frequency in Figure B-4. For frequencies higher than 0.1 Hz (wavelengths less than 18 m), the cup anemometer response is observed to fall off sharply. This response is consistent with the Climet anemometer's distance constant near 1.5 m.

A simple technique can be used to approximate the Equation (B-17) expression for anemometer cup overspeeding. This technique involves partitioning the scale effects multiplier into bands and assigning an average value of this multiplier to each band. The turbulence intensity contribution is also determined for each selected band. The sum of the products of the band-averaged scale

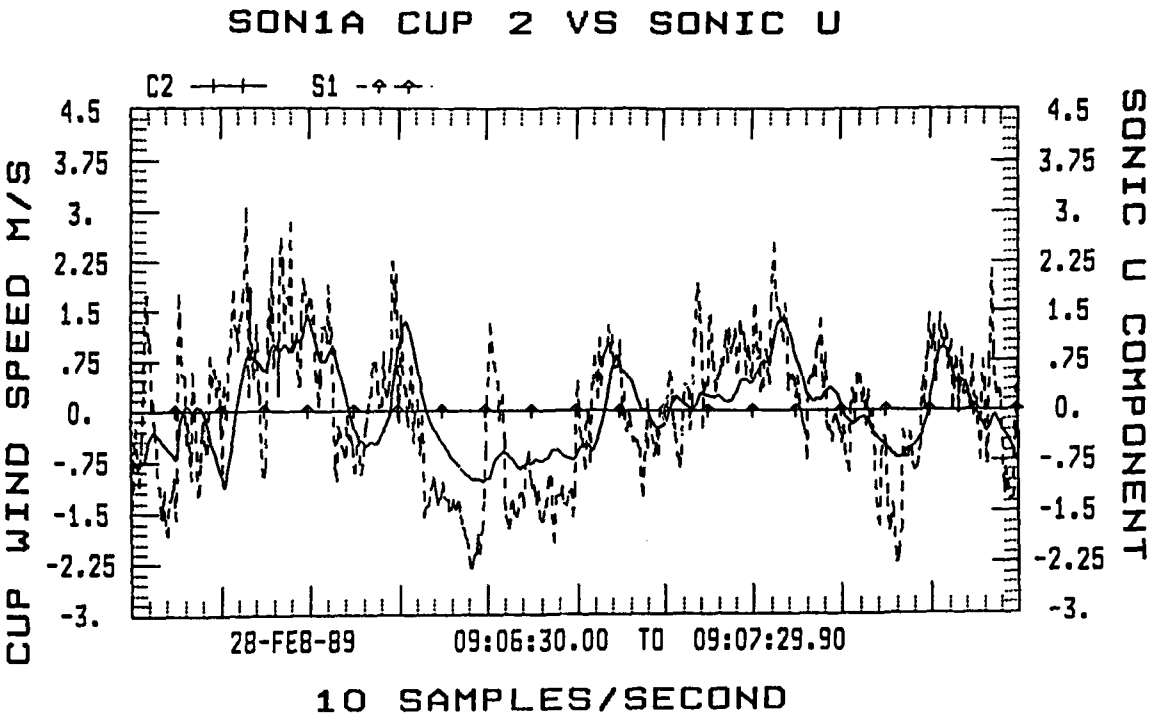

Figure B-3. Fluctuating Signal Components from a Climet Cup Anemometer (solid line) and a Sonic Anemometer (dashed line) in response to the Turbulent Wind Field Generated During a One Minute Segment of Data from Light Tunnel Trial 1. The Sampling Rate is 10 Hz.

effects multiplier with the turbulence intensity within each band becomes the horizontal turbulence contribution to anemometer cup overspeeding. A modified version of this approach is used to determine the vertical turbulence component contribution. The sum of horizontal and vertical contributions is the fractional anemometer cup overspeed estimate. The procedure is demonstrated in the following paragraphs, with the assumption that constants E and F are unity.

Wavelengths of the Light Tunnel data were normalized using Equation (B-15) and a λ_n of 1.5 m. Scale effects were then approximated using these normalized wavelengths. The scale effects multiplier illustrated in Figure B-1 can be partitioned into three step functions using Λ^* intervals ranging from 0.2 to 0.7, 0.7 to 12, and 12 to 40. The average multipliers for these ranges are 0.1, 0.45, and 0.1 respectively. More accurate representations of the scale effects multiplier can be obtained (at greater computational cost) using a greater number of intervals. However, the three chosen intervals serve for illustrative purposes in this report.

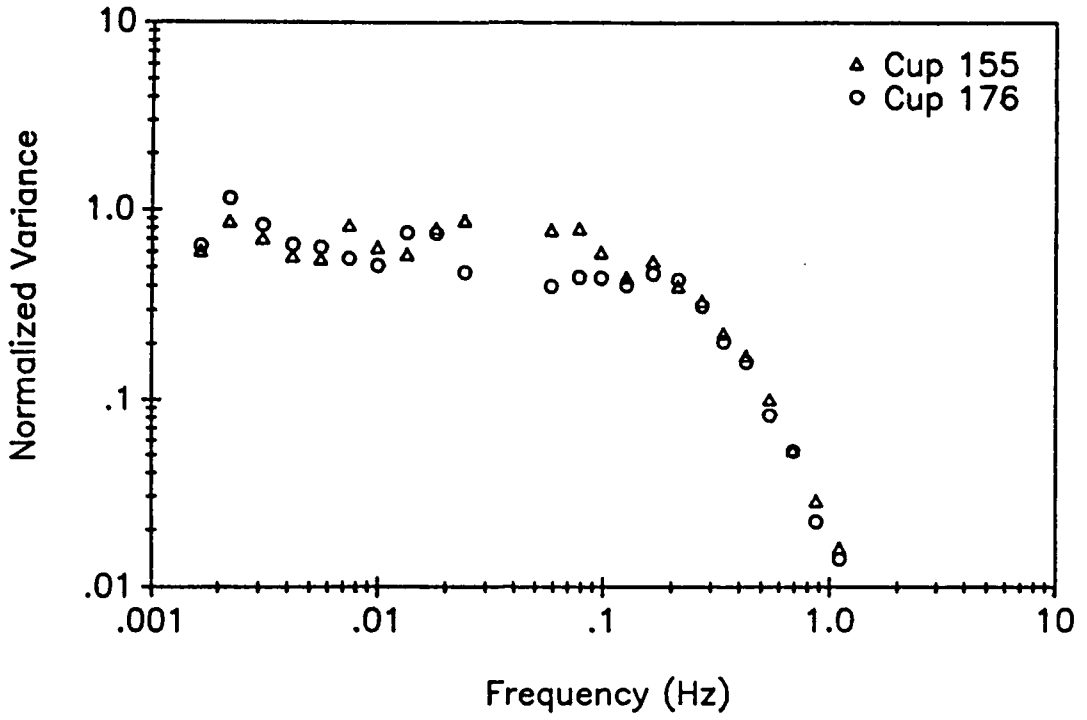

Figure B-4. Light Tunnel Study Average Cup Anemometer Variance Normalized by Sonic Anemometer Variance and Depicted as a Function of Frequency. Normalized Variance for Anemometer #155 is Represented by (x) and Anemometer #176 is Represented by (o).

Turbulence intensities were obtained by block averaging the Light Tunnel sonic anemometer data over frequency intervals that bound the selected step function bands. These frequency intervals were 5, 1.5, 0.1, and 0.025 Hz. Turbulence intensities within each band were obtained from successive differences (ΔI_x, ΔI_y) between adjacent band boundaries. The process is illustrated in Table B-2.

The Table B-2 turbulence intensity data, multiplied by the applicable scale multipliers, provide an estimate of fractional anemometer cup overspeeding. For the Trial 1 horizontal component only, the overspeeding contribution (OH) is

$$OH = 0.1x(.0077) + 0.45x(.0611) + 0.1x(.0264) = 0.031 \qquad (B\text{-}18)$$

or 3.1 percent. The comparable figure for Trial 2 is 3.4 percent.

Table B-2. Turbulence Intensities and Differences for Successive Averaging Intervals.

Averaging Interval (Hz)	Turbulence Intensity I_x	I_y	Intensity Differences ΔI_x	ΔI_y	$\Delta I_x^2+\Delta I_y^2$
		Trial 1: 0830-0854 MST			
5	0.563	0.282			
			0.073	0.049	0.0077
1.5	0.490	0.233			
			0.207	0.135	0.0611
0.1	0.283	0.098			
			0.151	0.060	0.0264
0.025	0.132	0.038			
		Trial 2: 0906-0930 MST			
5	0.573	0.286			
			0.049	0.062	0.0063
1.5	0.524	0.224			
			0.230	0.123	0.068
0.1	0.294	0.101			
			0.151	0.064	0.0269
0.025	0.143	0.037			

Estimation of the overspeed contribution by the vertical turbulence component is less certain. No direct measurements of the vertical turbulence intensity were made, and constant J of Equation (B-17) is unknown. However, the turbulence intensity in the crosswind direction was measured. For turbulence generated by a rotating circular fan it is reasonable to assume that the off-axis turbulence intensities in the crosswind and vertical directions were nearly the same. Also, the constant J is assumed to be nearly equal to H. With these assumptions, the scale effects multiplier estimates are 0.1, 0.7, and 0.95, and the vertical turbulence intensity overspeed contribution (OV) for Trial 1 is

$$OV = 0.1x(.049)^2 + 0.7x(.135)^2 + 0.95x(.06)^2 = 0.016 \qquad \text{(B-19)}$$

or 1.6 percent. The comparable figure for Trial 2 is 1.5 percent. The summed horizontal and vertical axis contributions to overspeeding were therefore estimated to be 4.7 percent for Trial 1 and 4.9 percent for Trial 2.

B.5. CONCLUSIONS

Cup anemometers are omnidirectional and are most often used to measure the scalar wind speed. In combination with a suitably matched wind vane, vector

wind component measurements can also be obtained. The sonic anemometer, on the other hand, measures wind components. A common product of horizontal wind component averages is the vector wind velocity. A different data processing technique can also be used with sonic anemometer data to calculate a scalar wind speed. A large percentage of the observed differences between sonic and cup anemometer wind measurements is due to DP differences. The data processing (DP) difference between vector and scalar wind measurements is not an error. Each data prossessing procedure has legitimate applications.

Differences in the performance of cup and sonic anemometers have been explored in some detail. Inherent differences between these instruments arise from exposure and inertial effects. The wake created by upstream transducers or support structures affects sonic anemometer wind component measurements, while cup anemometer exposure is usually unimpeded in all horizontal directions. Conversely, the sonic anemometer is virtually inertia free while the cup anemometer must gain or shed energy to achieve equilibrium with a non-steady flow. Performance uncertainties arise because both instruments are characterized in low turbulence wind tunnels, but are employed for measurements in the fully turbulent atmosphere.

The combined effects of turbulence scale and intensity must be known to determine the performance of cup and sonic anemometers in the turbulent atmosphere. Turbulence tends to disperse wake effects for sonic anemometers, improving their relative performance. No uncompensated angle of attack effects were found in the Light Tunnel trials, indicating that the wake effects compensation algorithm does a reasonable job of compensating for angular dependencies in the data. Conversely, cup anemometers can be precisely calibrated in wind tunnels, yet they overspeed in response to turbulence and/or any vertical wind component. Both instruments, therefore, have measurement biases. Sonic anemometers have speed- and orientation-dependent biases that must be corrected by transfer functions or lookup tables. The cup anemometer's overspeeding can be corrected if the interaction of turbulence scale and intensity with the anemometer's average distance constant is known. The major portion of cup anemometer overspeeding is in response to wavelengths shorter than 4π times the average distance constant.

Lockhart (1987) and Hayashi (1987) have independently determined that a cup anemometer's spin up distance constant is shorter than its spin down distance constant. Both of these numbers are needed to define an average distance constant. A cup anemometer's overspeed ratio can be computed when turbulence scales are normalized by this average distance constant. Virtually all scale effects that contribute to overspeeding lie within a band bounded by 0.2 and 40 Λ^* with the maximum effect occurring between 0.7 and 12 Λ^*.

A simple setup such as instruments downstream of a large fan in an open room can be used to obtain controlled turbulence measurements. If carefully characterized, this fan-generated wind field simulation can be used for instrument intercomparsion studies. The numerical results from the present study are considered approximations to be used for illustrative purposes because the instruments needed to do a detailed characterization were not at hand. However, these results show that major differences between cup and sonic anemometer measurements can be largely resolved by using appropriate DP algorithms and by accounting for turbulence scale and intensity effects on cup anemometers.

INTENTIONALLY BLANK

APPENDIX C.
STANDARD PRACTICE FOR MEASURING SURFACE WIND AND/OR TEMPERATURE BY SONIC MEANS

This appendix contains a draft ASTM standard that was prepared as part of this methodology investigation. The draft standard is intended for sonic anemometer users and addresses deployment, data reduction, siting to minimize interferences, calibration, and quality control. It is written in the ASTM standard format.

Standard Practice for
Measuring Surface Wind and/or Temperature
by Acoustic Means [1] (Second draft, 20 Feb 90)

1. Scope

1.1 This practice covers the measurement of vector wind components and/or virtual temperature by means of commercially available sonic anemometer/ thermometers that employ the inverse time measurement technique. This practice applies to the measurement of wind velocity components over horizontal flat terrain using instruments mounted on stationary towers. This practice also applies to speed of sound measurements that are converted to virtual temperatures but does not apply to the measurement of temperature by the use of ancillary resistance temperature devices.

1.2 This standard may involve hazardous materials, operations, and equipment. This standard does not purport to address all of the safety problems associated with its use. It is the responsibility of whoever uses this standard to consult and establish appropriate safety and health practices and determine the applicability of regulatory limitations prior to use.

2. Reference Documents

D 1356 Definitions of Terms Relating to Atmospheric Sampling and Analysis[2]

D 3670 Standard Practice for Determination of Precision and Bias of Committee D-22 Test Methods[2]

Standard Test Method for Determining the Performance of a Sonic Anemometer/ Thermometer(draft)[2]

D 4430 Standard Practice for Determining the Operational Comparability of Meteorological Measurements[2]

---

[1] This practice is under the jurisdiction of ASTM Committee D-22 on Sampling and Analysis of Atmospheres and is the direct responsibility of Subcommittee D22.11 on Meteorology.
Current edition approved _____. Published _____.

[2] Annual book of ASTM Standards, Vol. 11.03.

3. Terminology

3.1 Definitions:

3.1.1 Acceptance Angle (2α, deg)--The angular distance, centered on the anemometer's axis of symmetry, over which the following conditions are met: (a) wind components are unambiguously defined and (b) flow across the transducers is not seriously obstructed. Wind measurements using a sonic anemometer should be made within the acceptance angle.

3.1.2 Acoustic Pathlength (d, m)--The sum of the distance traveled by the acoustic wavefront from the transmitting to receiving transducers plus a correction for delays in the electronic circuit and transducers.

3.1.3 Increment of Velocity Resolution (Δv_i, m/s)--The largest change in an along-axis wind component that would not cause a change in the pulse arrival time count.

3.1.4 Sampling Period(s)--The record length or time interval over which data collection occurs.

3.1.5 Sampling Rate (Hz)--The rate at which data collection occurs, usually presented in samples per second or Hertz.

3.1.6 Sonic Anemometer/Thermometer--An instrument consisting of paired sets of acoustic transmitters and receivers, with a system clock and microprocessor circuitry to count intervals of time between transmission and reception of sound pulses. The fundamental measurement unit is transit time which, with a known transit distance or pathlength, is converted to velocity. Sonic anemometer output is a series of quasi-instantaneous velocity component readings along each axis and/or speed of sound. The speed of sound may be used to compute virtual temperature (T_v), and the velocity components may be averaged to describe the mean wind field or used to compute fluxes, turbulence intensities, and spectra.

3.1.7 Standard Error of the Velocity Estimate (Δv_n, m/s)--The increment of velocity resolution divided by the number of samples used to produce each

along-axis wind velocity measurement.

3.1.8 System Clock--The clock used for timing of acoustic pulses. The basic time pulse interval determines the instrument resolution.

3.1.9 System Delay (δt,μs)--The time delay through the transducer and electronic circuitry.

3.1.10 Thermodynamic Velocity Uncertainty (Δv_d, m/s)--Uncertainties in velocity due to the uncertainties of constants and variables used in the speed of sound equation.

3.1.10 Thermal Stability--A measure of the ability of the transducers and associated electronics to retain calibration over a range of operating temperatures.

3.1.11 Transducer Shadow Correction (v_{dm}/v_d)--The ratio of the "true" velocity v_{dm}, as measured in a wind tunnel or by another accepted standard, to the instrument along-axis wind measurement v_d. This is a transfer function used to compensate for the effects of along-axis flow shadowing by the transducers and their supporting structure.

3.1.12 Transit Time(t,s)--The time required for an acoustic wavefront to travel from the transducer of origin to the receiving transducer.

3.2 Symbols:

B	(dimensionless)	squared sums of sines and cosines of wind direction angle used to calculate wind direction standard deviation
c	(m/s)	speed of sound
d	(m)	acoustic pathlength
f	(dimensionless)	compressibility factor
t	(s)	time
T_v	(K)	virtual temperature

γ	(dimensionless)	specific heat ratio (c_p/c_v)
M	(erg/g K)	molar mass of air
n	(dimensionless)	sample size
R^*	(erg/mol K)	the universal gas constant
u	(m/s)	along-wind velocity component
u_s	(m/s)	velocity component along the array u axis
v	(m/s)	cross-wind velocity component
v_s	(m/s)	velocity component along the array v axis
WS	(m/s)	wind speed computed from measured velocity components
Δt	(s)	clock pulse resolution
Δv_d	(m/s)	thermodynamic velocity uncertainty
Δv_n	(m/s)	standard error of the velocity estimate
Δv_i	(m/s)	increment of velocity resolution
δt	(μs)	system delay
Θ	(deg)	mean wind direction
Θ_r	(deg)	wind direction measured in degrees clockwise from the sonic anemometer $+v_s$ axis to the along-wind u axis
ϕ	(deg)	orientation of the sonic anemometer axis with respect to the true north
σ_Θ	(deg)	standard deviation of wind azimuth angle
subscript i		the ith individual measurement

4. Summary of Practice

4.1 A calibrated sonic anemometer/thermometer is installed, leveled, and oriented into the wind to ensure that the measured along-axis velocity component falls within the instrument's acceptance angle.

4.2 The wind components measured over a user-defined sampling period are averaged and subjected to a software rotation into the mean wind. This

rotation maximizes the mean along-axis wind component and reduces the mean cross-component to zero.

4.3 Mean wind speed and direction are computed.

4.4 For the sonic anemometer/thermometer, the speed of sound solution is obtained and converted to a virtual temperature.

4.5 The mean components, variances, and covariances are computed.

5. Significance and Use

Sonic anemometer/thermometers are the instruments of choice for the measurement of turbulent components of the atmosphere except for confined areas and very close to the ground (1).[3] This practice applies to the use of these instruments for field measurement of the wind, virtual temperature, and atmospheric turbulence components. The quasi-instantaneous velocity component measurements are averaged over user-selected sampling times to define mean along-axis wind components, mean wind speed and direction, and the variances and/or covariances of individual components or component combinations. Covariances are used for eddy correlation studies and for computation of boundary layer heat and momentum fluxes. The sonic anemometer/thermometer provides the data required to characterize the boundary layer for dispersion modeling, environmental monitoring, and weather analysis and forecasting.

6. Interferences

6.1 Mount the sonic anemometer probe for an acceptance angle into the mean wind. Wind velocity components from angles outside the acceptance angle may be subject to flow blockage effects from the transducers and supporting structure, or may not be unambiguously defined. Obtain acceptance angle information from the manufacturer.

---

[3]The boldface numbers in parentheses refer to the list of references at the end of this practice.

6.2 Mount the sonic array at a sufficient distance from reflecting surfaces to prevent acoustic reflections. A separation distance of at least 1 m is recommended.

6.3 To obtain representative samples of the mean wind, the sonic array must be exposed at a representative site. For synoptic and general environmental monitoring purposes, wind is measured over level, open terrain at a height of 10 m above the ground. Surface roughness and displacement distance should be considered in the site selection process. Select a sufficient measurement height that the dominant turbulence scale exceeds the acoustic pathlength by a factor of at least 2π.

6.4 Carefully measure and verify array tilt and alignment. The vertical component of the wind is usually much smaller than the horizontal components. Therefore, the vertical wind component is highly susceptible to cross-component contamination from tilt angles not aligned to the terrain slope. Momentum flux computations are particularly susceptible to off-axis contamination **(2)**. Calculations and transformations (Section 11) for sonic anemometer data are based on the assumption that the mean vertical velocity ($\overline{w}$) is zero. Arrays mounted on a sloping surface may require tilt angle adjustments. Also, avoid mounting the array close (within 2 m) to the ground surface where velocity gradients are large and $\overline{w}$ may be nonzero.

6.5 Sonic anemometer transducers are tiny microphones and are therefore sensitive to extraneous noise sources, especially ultrasonic sources at the anemometer's operating frequency. Mount the transducer array in an environment free of extraneous noise sources.

6.6 Sonic anemometer transducer arrays contribute a certain degree of blockage to flow. Consequently, the manufacturer should supply a transducer shadow correction algorithm as part of the data processing algorithms.

7. Apparatus

The appartus includes a sonic anemometer/thermometer that makes use of the inverse transit time solution, its calibration chamber, a leveling device, calipers, and a readout device. These instruments measure wind components

and/or the speed of sound along 1, 2, or 3 axes.

8. Sampling

8.1 The basic sampling rate of a sonic anemometer is on the order of several hundred Hz. These raw transit times are averaged within the instrument's software to produce basic measurements at a rate of 10 to 20 Hz, which may be user-selectable. This sampling is done to improve instrument measurement precision and to suppress high frequency noise and aliasing effects. The 10 to 20 Hz sample output in a serial digital data stream or through a digital to analog converter is the basic increment of measurement for a sonic anemometer.

8.2 The sampling time must be sufficiently long to obtain statistically stable measurements of the phenomena of interest within the constraints of a data collection system's capabilities. To obtain representative results, perform sampling over periods where flow conditions are nearly homogeneous in space and stationary in time. Sampling periods on the order of 15 minutes usually generate sufficient data to describe the turbulent state of the atmosphere. Sampling periods in excess of one hour may contain undesired trends in wind direction.

9. Calibration

9.1 Prior to calibration, measure the transducer spacing with calipers to a precision of 1 mm or greater, depending on the manufacturer's calibration requirements. Records of transducer spacing for each sonic anemometer array shall be kept on file for reference. Internal alignment of the instrument shall be within ± 1 deg for mean and variance measurements. Internal alignment to within ± 0.1 deg is recommended for sonic anemometers used for momentum flux calculations (2).

9.2 Calibrate sonic anemometers in a zero wind chamber (Figure 1). This chamber is an acoustically damped enclosure of known temperature where air motions are minimal. Chamber temperature measured with a resolution of 0.1°C and a precision of ± 0.5°C or better is required to provide a zero-velocity reference. Dessicant shall be used in the chamber to control humidity. Note: The instrument's carrying case may serve as a zero wind chamber. Consult the manufacturer for specific information on the zero wind chamber and calibration

procedures.

9.3 The sonic anemometer should retain its calibration over its range of thermal stability unless the acoustic pathlength changes. Recalibration is needed after changing transducers or electronics components or adjusting transducer spacing. Calibration is required prior to deployment of the instrument for field measurements and for verification after the measurement process is completed. Calibrate instruments at least every 6 months.

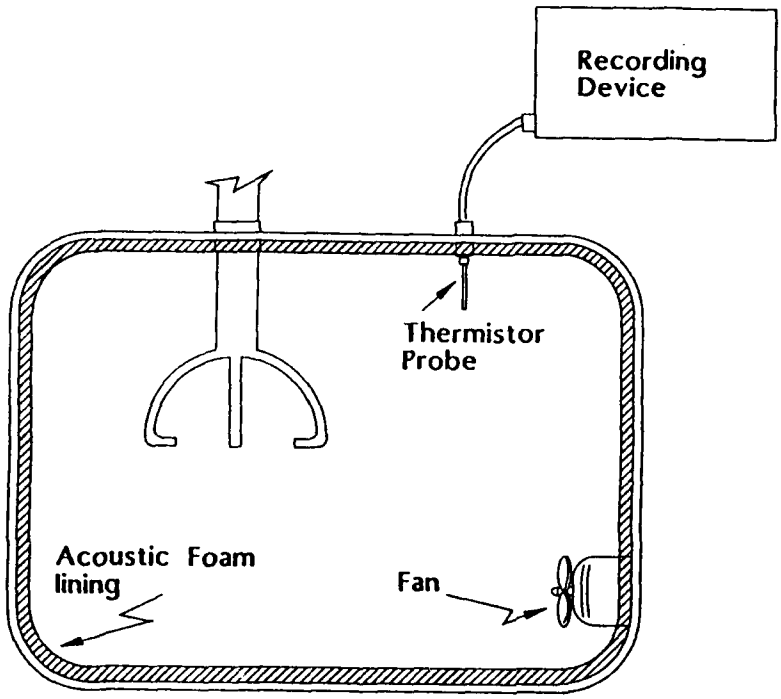

Figure 1. A sonic anemometer calibration chamber.

10. Procedure

10.1 Mount a recently calibrated sonic anemometer on a solid, vibration-free platform free of the interferences described in Section 6.

10.2 Select an orientation into the mean flow within the instrument's acceptance angle. Record the orientation angle to within ±1 deg. Use a leveling device to level the transducer head to within ±0.25 deg of vertical or the requires slope angle.

10.3 Install cabling to the recording device, keeping cabling isolated from other electronics noise sources or power cables to minimize inductance or crosstalk.

10.4 Collect data over an extended sampling period (1-hour recommended) during representative operating conditions. Examine the data for extraneous noise, alignment faults, or other malfunctions. Note: Deviation of the mean vertical velocity from zero should not exceed the desired measurement precision. Alignment and/or data reduction software modifications not addressed in this Practice may be needed for locations where $\bar{w}$ is nonzero.

10.5 Measurements made for the purpose of calculating variances or covariances should not include significant wind excursions from the acceptance angle range and should not include periods of significant wind meandering or trends.

11. Calculations and Transformations

11.1 Each sonic anemometer provides wind component measurements with respect to a coordinate system defined by its array axis. Each array design requires specific calculations and transformations to convert along-axis measurements to the desired wind component data. The calculations and transformations presented in Section 11 of this practice are applicable to orthogonal arrays. Reference 3 provides comparable information for a common non-orthogonal array. Obtain specific calculations and transformation equations from the manufacturer.

11.2 Figure 2 illustrates a coordinate system applicable to orthogonal array sonic anemometers. The wind component sign convention is as follows:

(a) An along-axis wind component entering the array from the front will have a positive sign ($+u_{si}$).

(b) A cross-axis wind component entering the array from the left will have a positive sign ($+v_{si}$).

(c) A vertical wind component entering the array from the bottom will have a

positive sign ($+w_{si}$).

The subscript s refers to a wind component measured with respect to the sonic array axes, and the subscript i refers to the ith individual measurement. Array orientation (ϕ) is measured clockwise from true north, as illustrated in Figure 2.

11.3. Sonic anemometers employing the inverse time (1/t) measurement technique obtain velocity by subtracting the inverse transit times of acoustic pulses traveling in opposite directions along an acoustic path. A quasi-instantaneous along-axis velocity component is given by

$$u_{si} = \frac{d}{2}\left[\frac{1}{t_1} - \frac{1}{t_2}\right] \qquad (1)$$

where d is the acoustic pathlength and t_1 and t_2 are the along-axis acoustic pulse transit times. Similar equations provide cross-axis and vertical axis velocity components.

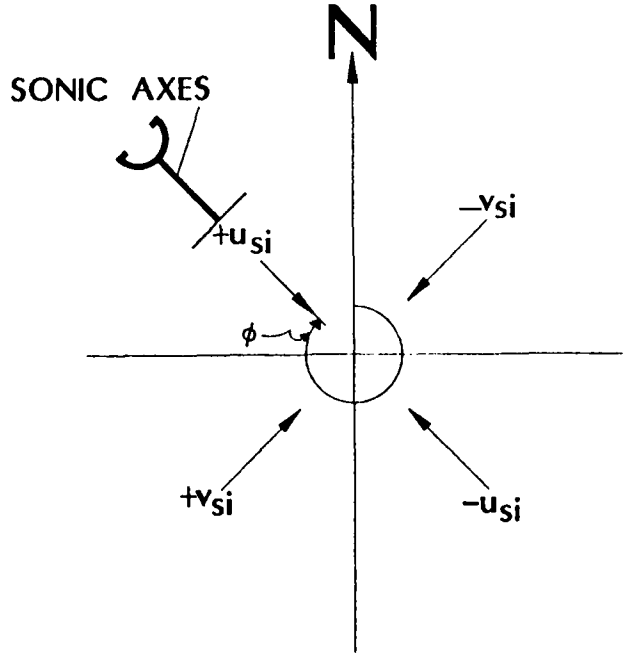

Figure 2. A sonic anemometer array coordinate system.

11.4 The data of interest for sonic anemometer wind measurement will often be the mean wind speed and direction, and/or the individual components that are used to calculate variances and covariances. A coordinate rotation is required to obtain these data from the measured u_{si} and v_{si}.

11.5 Mean wind speed ($\overline{WS}$). Mean wind speeds of interest may be the vector wind speed required for trajectory calculations, or the scalar wind speed required for dispersion modeling. The horizontal vector mean wind speed is defined as the square root of the sum of the squares of mean along-axis and cross-axis horizontal velocity components. That is, for a user-defined time interval,

$$\overline{WS}\ (\text{vector}) = [(\bar{u}_s)^2 + (\bar{v}_s)^2)]^{1/2}, \tag{2}$$

where $\bar{u}_s$ and $\bar{v}_s$ are the mean along- and cross-axis wind components defined by

$$\bar{u}_s = \frac{1}{n}\left(\sum_{i=1}^{n} u_{si}\right) \tag{3}$$

$$\bar{v}_s = \frac{1}{n}\left(\sum_{i=1}^{n} v_{si}\right) \tag{4}$$

Sample size is represented by n. The scalar mean horizontal wind speed is the sum of the square root of the sum of the squares of each individual horizontal velocity component divided by sample size.

$$\overline{WS}\ (\text{scalar}) = \frac{1}{n}\left(\sum_{i=1}^{n} [u_{si}^{\ 2} + v_{si}^{\ 2}]^{1/2}\right) \tag{5}$$

11.6 Mean Wind Direction. An ANSI FORTRAN two-argument arctangent function ATAN2D is used to define a rotated mean wind direction θ_r measured in degrees clockwise from the $+v_s$ array axis to the along wind (u) axis as

$$\bar{\theta}_r = \text{ATAN2D}\ (\bar{u}_s/\bar{v}_s) \tag{6}$$

The mean wind direction $\bar{\theta}$, defined with respect to true North, is obtained by adding θ_r to the sonic anemometer axis orientation (ϕ) minus 90°

$$\bar{\theta} = \bar{\theta}_r + \phi - 90° \tag{7}$$

11.7 The standard deviation of the wind azimuth angle (σ_θ) is calculated in a computationally-efficient manner using

$$\sigma_\theta = \arcsin[(1-B^2)^{0.5}] \tag{8}$$

where B^2 is obtained from sines and cosines of individual wind angles

$$B^2 = \left[\frac{1}{n}\sum_{i=1}^{n} \sin\theta_{si}\right]^2 + \left[\frac{1}{n}\sum_{i=1}^{n} \cos\theta_{si}\right]^2 \tag{9}$$

To achieve a representative sample size while minimizing the influences of long term wind-direction trends on σ_θ, 15-min σ_θ calculations are recommended (3).

11.8 The mean alongwind and crosswind components are defined in terms of $\bar{\theta}_r$ as

$$\bar{u} = \bar{u}_s \sin\bar{\theta}_r + \bar{v}_s \cos\bar{\theta}_r \tag{10}$$

$$\bar{v} = \bar{u}_s \cos\bar{\theta}_r + \bar{v}_s \sin\bar{\theta}_r = 0 \tag{11}$$

11.9 Sonic anemometer/thermometers employing the inverse time measurement technique obtain a speed of sound solution (usually on the vertical axis) using the sum of the inverse transit times of acoustic pulses traveling in opposite directions along are acoustic path. A quasi-instantaneous solution for speed

of sound is

$$c = \frac{d}{2}\left(\frac{(t_1 + t_2)}{2t_1t_2\cos\alpha}\right) \tag{12}$$

the $\cos\alpha$ term takes into account the deflection of an acoustic wavefront by the wind component normal to the acoustic path. For a measurement made on the vertical axis, this factor is a function of the horizontal wind speed.

$$\cos\alpha = \cos\left(\sin^{-1}((u_{si}^2 + v_{si}^2)^{0.5}/c)\right) \tag{13}$$

A virtual temperature (T_v) solution is obtained from the speed of sound equation

$$T_v = \frac{Mc^2}{\gamma f R^*} \tag{14}$$

where M is the molar mass of the air, γ is the specific heat ratio, f is the compressibility factor, and R^* is the universal gas constant. M, γ, and f are slowly varying functions of temperature and humidity.

11.10 Variances and covariances for orthogonal arrays can be computed using $\bar{\theta}_r$, T_v, and the unrotated u_s and v_s. Commonly used variances (covariances) are given by the mean of the squares (mean of the products) minus the square of the individual means (product of the means), as defined below. Note that products of means containing $\bar{v}$ are zero.

Alongwind velocity variance: $\overline{u'u'} = (\overline{uu}) - (\bar{u})(\bar{u})$

$$= (\overline{u_s u_s})\sin^2\bar{\theta}_r + 2(\overline{u_s v_s})\sin\bar{\theta}_r\cos\bar{\theta}_r + \overline{v_s v_s}\cos^2\bar{\theta}_r$$

$$- (\overline{u_s})(\overline{u_s})\sin^2\bar{\theta}_r - 2(\overline{u_s})(\overline{v_s})\sin\bar{\theta}_r\cos\bar{\theta}_r - (\overline{v_s})(\overline{v_s})\cos^2\bar{\theta}_r \tag{15}$$

Crosswind velocity variance: $\overline{v'v'} = (\overline{vv})$

$$= (\overline{v_s v_s})\sin^2\bar{\theta}_r - 2(\overline{u_s v_s})\sin\bar{\theta}_r\cos\bar{\theta}_r + (\overline{u_s u_s})\cos^2\bar{\theta}_r \tag{16}$$

Vertical velocity variance: $\overline{w'w'}=(\overline{ww})-(\bar{w})(\bar{w})$ (17)

Covariance of alongwind and vertical velocities (stress): $\overline{u'w'}=(\overline{uw})-(\bar{u})(\bar{w})$

$$= (\overline{u_s w})\sin\bar{\theta}_r + (\overline{v_s w})\cos\bar{\theta}_r - (\bar{u}_s)(\bar{w})\sin\bar{\theta}_r - (\bar{v}_s)(\bar{w})\cos\bar{\theta}_r \quad (18)$$

Covariance of virtual temperature (T_v) and vertical velocity:

$$\overline{w'T_v'} = (\overline{wT_v}) - (\bar{w})(\overline{T_v}) \quad (19)$$

Covariance of alongwind and crosswind velocities: $\overline{u'v'}=(\overline{uv})$

$$= (\overline{u_s v_s} - \overline{v_s v_s})\sin\bar{\theta}_r \cos\bar{\theta}_r + \overline{u_s v_s} \cos^2\bar{\theta}_r \quad (20)$$

12. Measurement Resolution and Uncertainty

12.1 The performance of a sonic anemometer/thermometer is determined by instrument resolution and uncertainty. Following ASTM D3670 and D4430, the increment of resolution is the smallest change in an atmospheric variable that is reported as a change in the measurement, while uncertainty is defined in terms of systematic difference (bias), operational comparability, and standard deviation of measurement differences (precision). Resolution is determined by the anemometer electronics, while bias, comparability, and precision are defined by instrument intercomparison testing, as described in ASTM XXXX. For temperature measurement, additional uncertainties are introduced through thermodynamic variables used in the speed of sound equation.

12.2 System resolution is limited by the resolution of the internal clock counting interval (Δt). The effect of clock resolution on velocity resolution (Δv_i) is

$$\Delta v_i = \frac{d\ \Delta t}{2\ t^2} \quad (21)$$

where t is a nominal transit time between transducer pairs in a zero wind field

and Δt is the inverse of the clock rate in Hertz. A change in wind speed of less than Δv_i m/s would not cause a change in the pulse arrival time count. Consequently, this is the measurement system's single pulse increment of velocity resolution. Note: If the transit times are not measured simultaneously, as in existing single transducer pair sonic anemometers, the uncertainty is doubled. Additional counting circuit uncertainties can arise when the counter is started or stopped. Consult the manufacturer for specific information on counting circuitry and velocity resolution.

12.3 Sonic anemometers typically transmit up to several hundred pulses per second, with arithmetic averaging used to produce measurements at a rate of 10 or 20 Hz. The distribution of Δv_i within each averaging period is considered to be random. Consequently, the standard error of the velocity estimate (Δv) is improved by the square root of the number of readings (n) used in the averaging.

$$\Delta v_n = \Delta v_i / \sqrt{n} \tag{22}$$

12.4 Sonic anemometer system electronics precision is affected by delay (δt) through the transducers and electronic circuitry and by the precision (δd) with which d is known. The system delay, on the order of 10μs, is added to the transit times in both directions (5). For a velocity component measurement, the effect is

$$v + \delta v = \frac{(d + \delta d)}{2} \left[\frac{1}{(t_1 + \delta t)} - \frac{1}{(t_2 + \delta t)} \right], \tag{23}$$

where δv is the uncertainty due to the cumulative effects of δd and δt. The combined effects of δd and δt are determined by acoustic pathlength measurements (see ASTM XXXX). Consult the manufacturer for information on the method used to determine system delay and its effects on measurement uncertainty.

12.5 Uncertainty of virtual temperature (T_v) computation is affected by uncertainties of thermodynamic constants used in the speed of sound equation (Section 11.9). These constants are the universal gas constant (R^*), the

specific heat ratio (γ), the compressibility factor (f), and molecular weight of air (M). The uncertainties, computed for standard atmospheric temperature and pressure conditions, represent differences and uncertainties in the constants as found in standard references used in the United States, Canada, the Soviet Union, and the United Kingdom. The cumulative effects of thermodynamic uncertainties create an uncertainty in T_v of $\pm 0.6\%$. An uncertainty of this magnitude renders sonic computation of absolute T_v unsuitable for most applications. However, the mean T_v is subtracted from indivudual readings to produce a fluctuating component used in temperature variance and covariance computations. Because thermodynamic uncertainties are virtually identical for the mean and individual readings, the process of subtraction effectively removes this source of error. System clock resolution and electronics precision, which is on the order of 0.01%, is the remaining source of uncertainty (6).

12.6 Thermodynamic uncertainties are introduced through the speed of sound equation (Equation 14) to along-axis wind measurements by the calibration procedure. The product of constants $\gamma FR^*/M$ has nominal magnitude of 403.24 with an uncertainty of 1% over a normal range of temperature and humidity in the atmosphere. This uncertainty can be reduced to 0.2% by controlling humidity within the calibration chamber and by performing calibration at room temperature. The remaining variable, T_v, is usually known to within one degree Celsius. The speed of sound obtained from Equation 14 is used (with stored information on system delay) to determine the acoustic pathlength (d).

$$d = 2c \left[\frac{1}{t_1} + \frac{1}{t_2} \right]^{-1}$$

The thermodynamic uncertainty is carried through to Equation 1, creating an uncertainty in measured wind speed (Δv_d) of approximately 0.01 m/s for each meter per second of along-axis wind. The total along-axis wind component measurement uncertainty (Δv) is the sum of this speed-dependent uncertainty plus the standard error of the velocity estimate described in Section 12.3 (6).

$$\Delta v = \Delta v_d \times v_d + \Delta v_n \qquad (24)$$

Note: Sonic anemometer performance is verified by intercomparison tests, where results are reported in terms of bias, comparability, and precision.

13. References

(1) Kaimal, J. C., 1979: Sonic anemometer measurement of atmospheric turbulence. Proc. Dynamic Flow Conference, Skovlinde, Denmark, DISA Electronic A/S, 551-565.

(2) Kaimal, J. C. and D. A. Haugen, 1969: Some errors in the measurement of Reynolds stress. J. Appl. Meteor., 8, 460-462.

(3) Wyngaard, J. C., and S. F Zhang, 1985: Transducer-shadow effects on turbulence spectra measurec by sonic anemometers. J. Atmos. and Oceanic Tech., 2, 548-558.

(4) EPA, 1987b: On-site meteorological program guidance for regulatory modeling applications, EPA-450/4-87-013, Office of Air Quality Planning and Standards. Research. Triangle Park, NC 27711.

(5) Coppin, P. A., and K. J. Taylor, 1983: A three component sonic anemometer/thermometer system for general micrometeorological research. Boundary Layer Meteor., 27, 27-42.

(6) Biltoft, C. A., 1987: Final Report Development of sonic anemometer software. U.S. Army Dugway Proving Ground DPG-FR-88-702 (AD-B120769).

APPENDIX D.
STANDARD TEST METHOD FOR DETERMINING THE PERFORMANCE OF A SONIC ANEMOMETER/THERMOMETER

The appendix contains a draft ASTM standard that was prepared as part of this methodology investigation. The draft standard is intended for use by manufacturers and testing laboratories to characterize the performance of sonic anemometers. It is written in the ASTM standard format.

Standard Test Method for
Determining the Performance
of a sonic Anemometer/Thermometer[1]

1. Scope

1.1 This method covers the determination of the:

acoustic pathlength
increment of resolution
standard error of the velocity estimate
transducer shadow correction
velocity calibration range
thermal stability range

of a sonic anemometer which employs the inverse time measurement technique for velocity and/or speed of sound.

1.2 This method applies to laboratory and wind tunnel calibration of sonic anemometers which utilize the inverse time (1/t) measurement technique for velocity and/or speed of sound. The increment of resolution and standard error of the velocity estimate are defined by the clock rate, sampling, and averaging techniques chosen by the manufacturer. The acoustic pathlength is determined from precise measurements of transducer separation distance and system delay. The transducer shadow correction and velocity calibration range are influenced by the scale and intensity of the turbulent flow around the anemometer array and may vary from the laboratory to the free atmosphere. Use of transfer functions derived from wind tunnel data in the atmosphere must be done with an understanding of the differences in turbulence scale and intensity between the wind tunnel and the atmosphere. Intercomparison tests conducted in the turbulent atmosphere are used to verify performance. This method does not apply to the measurement of temperature by the use of ancillary resistance temperature devices attached to anemometer arrays.

---

[1]This method is under the jurisdiction of the ASTM Committee D-22 on Sampling and Analysis of Atmospheres and is the direct responsibility of Subcommittee D-22.11 (Meteorology).

1.3 This standard may involve hazardous materials, operations, and equipment. This standard does not purport to address all of the safety problems associated with its use. It is the responsibility of whoever uses this standard to consult and establish appropriate safety and health practices and determine the applicability of regulatory limitations prior to use.

2. Applicable Documents

C 384 Standard Test Method for Impedance and Absorption of Acoustical Materials by the Impedance Tube Method[2]

D 1356 Definitions of Terms Relating to Atmospheric Sampling and Analysis[3]

D 3670 Standard Practice for Determination of Precision and Bias of Committee D-22 Test Methods[3]

D 4430 Standard Practice for Determining the Operational Comparability of Meteorological Measurements[3]

E 177 Practice for Use of Terms Precision and Bias in ASTM Test Methods[4]

E 380 Standard Practice for Use of the SI International System of Units[3]

3. Summary of Methods

3.1 This method requires the following equipment as described in Section 6: (a) a zero Wind Chamber, (b) a pathlength chamber with pressurized gas sources and associated plumbing, and (c) a wind tunnel with a minimum working area (test section) diameter of twice the longest sonic anemometer array dimension.

---

[2]Annual Book of ASTM Standards, Vol. 4.06.

[3]Annual Book of ASTM Standards, Vol. 11.03.

[4]Annual Book of ASTM Standards, Vol. 14.02.

3.2 Use the clock rate, sampling, and averaging procedures to define the increment of resolution (Δv_i) and the standard error of the velocity estimate (Δv_n).

3.3 Determine the acoustic pathlength (d) through precise measurement of transducer separation distance and system delay contributions. This is accomplished through precise measurements with calipers or a specially constructed jig, or through measurements in a pathlength chamber using nitrogen and argon gases.

3.4 Determine the range of thermal stability through a series of readings taken over a desired temperature range in a zero wind calibration chamber.

3.5 Define the velocity calibration range (Uc to Us) using a wind tunnel.

3.6 Mount the transducer array on a rotating plate in a wind tunnel and measure transducer shadow effects as a function of axis orientation.

3.7 Calculate a transfer function from information derived in procedure 3.6 and include the transfer function algorithm in system software. Repeat procedure 3.6 to verify the transfer function.

3.8 Verify performance through intercomparison tests in fully turbulent conditions, where results are reported in terms of bias, comparability, and precision.

3.9 Repeat procedures 3.3 through 3.8 for a representative sample of each type or model of sonic anemometer/thermometer. Report test results.

4. Significance and Use

This method provides a standard for comparison of sonic anemometers that use inverse time solutions for velocity and/or speed of sound. It provides an unambiguous determination of instrument resolution, transfer function, calibration range, and thermal stability. The procedures outlined in Section 9 are applicable to manufacturers for the purpose of describing the performance of

their products, and to major instrumentation test facilities for the purpose of verifying manufacturers' claims. Note: This procedure does not address transducer sensitivity to moisture. Manufacturers shall provide this additional information.

Instrument users should perform calibration checks as specified by the manufacturer prior to use and frequently during use. A standard practice for measuring surface wind and/or temperature by sonic means is described in ASTM (draft).

5. Terminology

5.1 Definitions:

5.1.1 Acoustic Pathlength (d, m)--The physical distance between transducer transmitter-receiver pairs (transducer separation distance) plus an adjustment for the system delay (δt).

5.1.2 Critical Reynolds number--The Reynolds number at which an abrupt decrease in an object's drag coefficient occurs.

5.1.3 Calibration Range (U_c to U_s, m/s)--The range of velocity between creeping flow and the flow at which a critical Reynolds number (Rc) is reached. The calibration range defines the velocity or Re range over which the anemometer array's drag coefficient (C_D) remains constant. The drag coefficient varies as a function of Re at very low speed (creeping) flows and at high speed flows above Rc **(1)**.[5]

5.1.4 Increment of Velocity Resolution (Δv_i, m/s)--The largest change in an along-axis wind compoennt that would cause no change in the pulse arrival time count.

5.1.5 Reynolds Number (Re)--The non-dimensional ratio of inertial to viscous forces based on the characteristic dimension of an object immersed in a flowing fluid, the fluid velocity, and viscosity.

---

[5]The boldface numbers in parentheses refer to the list of references at the end of this practice.

5.1.6 Sonic Anemometer/Thermometer--An instrument consisting of paired sets of acoustic transmitters and receivers, with microprocessor circuitry to count intervals of time between transmission and reception of sound pulses. The fundamental measurement unit is transit time which, with a known transit distance or pathlength, is converted to velocity. Sonic anemometer performance is a function of clock time resolution (described by the increment of velocity resolution), precision of acoustic pathlength determination, and transfer functions which describe the interaction of the sonic anemometer with the velocity field in which it is immersed. Sonic anemometer output is a series of quasi-instantaneous velocity component readings along each axis and/or the speed of sound. The speed of sound may be used to compute virtual temperature, and the velocity components may be averaged to describe the mean wind field or used to compute fluxes, turbulence intensities, and spectra.

5.1.7 Speed of Sound--Propagation velocity of an adiabatic compression wave through gas.

$$c = (\partial P/\partial \rho)_s^{1/2} \qquad (1)$$

where P is pressure, ρ is density, and subscript s refers to an isentropic (adiabatic) process(2). The velocity of the compression wave defined along each axis of a Cartesian coordinate system is the sum of propagation velocity c plus the motion of the gas along that axis. For estimation purposes in this method, a nominal value of 340 m/s is used for speed of sound in still air.

5.1.8 System Clock--The clock used for timing of acoustic pulses. The basic time pulse interval determines the instrument resolution. A minimum clock stability of 0.01% over a temperature range of -20°C to +70°C is required.

5.1.9. System Delay (δt, μs)--The time delay through the transducer and electronic circuitry (3).

5.1.10 Standard Error of the Velocity Estimate (Δv_n, m/s)--The increment of velocity resolution divided by the number of samples used to produce each along-axis wind velocity measurement.

5.1.11 Thermal Stability Range--A measure of the ability of the transducers and associated electronics to retain calibration over a range of operating temperatures.

5.1.12 Time Resolution (Δt,μs)--Resolution of the internal clock used to measure time.

5.1.13 Transducer Shadow Correction (v_{dm}/v_d)--The ratio of the "true" velocity v_{dm}, as measured in a wind tunnel or by another accepted standard, to the instrument along-axis wind measurement v_d. This is a transfer function used to compensate for the effects of flow shadowing by the transducers and their supporting structure.

5.1.14 Transfer Function (dimensionless)--The relationship of a measurement system's output to the input signal or energy. For a sonic anemometer/ thermometer, it is the transducer shadow correction. Spectral transfer functions, which include effects of line averaging and path separation, are beyond the scope of this method (4).

5.1.15 Transit Time (s)--The time interval for transmission and reception of a sound pulse between a transmitter-receiver pair. Transit time is related to the speed of sound c and the along-axis (v_d) and cross-axis (v_n) wind components by (5)

$$t = \left[\frac{(c^2 - v_n^2)^{1/2} \pm v_d}{c^2 - (v_d^2 + v_n^2)}\right]d \qquad (2)$$

where d is the acoustic pathlength. Transit time differences from one direction (t_1, computed for $+v_d$) to the other (t_2, computed for $-v_d$) for each transducer pair are determined by the magnitude of the along-axis (v_d) component. Inverse transit times are used with transit distance (d) to produce velocity and speed of sound solutions. The inverse transit time solution for velocity is

$$v_d = \frac{d}{2}\left[\frac{1}{t_1} - \frac{1}{t_2}\right] \qquad (3)$$

and the inverse transit time solution for speed of sound is

$$c = \frac{d}{2}\left[\frac{t_2 + t_1}{t_1 t_2 \cos\alpha}\right] \qquad (4)$$

The $\cos\alpha$ term in Equation (4) takes into account the deflection of acoustic waves by the wind component normal to the acoustic path. For a speed of sound measurement made along the vertical axis, α is given by

$$\alpha = \sin^{-1}\left((V_n^2 + V_d^2)^{0.5}/c\right) \qquad (5)$$

5.1.16 Turbulence Scale--The dimension or scale of the dominant turbulence component in the flow.

5.2 Symbols:

c	(m/s)	speed of sound
c_p	(erg/g K)	specific heat at constant pressure
c_v	(erg/g K)	specific heat at constant volume
d	(m)	acoustic pathlength
f	(dimensionless)	compressibility factor
M	(g/mol)	molecular weight of a gas
P	(mb)	pressure
R^*	(10^4erg/mol K)	universal gas constant
Rc	(dimensionless)	Critical Reynolds number
Re	(dimensionless)	Reynolds number
t	(s)	time
T	(K)	absolute temperature
T_v	(K)	virtual temperature
U_c	(m/s)	upper limit for creeping flow
U_s	(m/s)	Critical Reynolds number velocity
v_d	(m/s)	along-axis wind component as measured by the sonic anemometer
v_{dm}	(m/s)	wind tunnel along-axis wind component ($v_t \cos\theta$)
v_n	(m/s)	cross-axis wind component as measured by the sonic anemometer
v_t	(m/s)	wind tunnel measured velocity
Δ	----	an unbiased increment
δt	(μs)	system delay
γ	(dimensionless)	specific heat ratio (c_p/c_v)
Δv_i	(m/s)	increment of velocity resolution
Δv_n	(m/s)	standard error of the velocity estimate
θ	(deg)	sonic probe orientation into the mean flow

6. Apparatus

6.1 Zero Wind Chamber. A zero wind chamber is used to calibrate the sonic anemometer/thermometer. The chamber must be sized to fit the sonic anemometer array and accommodate a temperature probe (see Figure 1). The chamber must be lined with acoustic foam and designed to minimize thermal gradients and acoustic reflections. An acoustic foam lining with a sound absorption coefficient of 0.8 or better at 6300 Hz as determined by ASTM C-384 is recommended. A small fan may be used to establish thermal equilibrium within the chamber before a zero wind calibration is made.

6.2 Pathlength Chamber:

6.2.1 The pathlength chamber is designed to fit and seal an axis of the array for acoustic pathlength determination. Gas chamber components must be designed using non-expanding, non-outgassing materials such as Kevlar.[6] O-ring seals made of non-outgassing materials are recommended to prevent pressure loss and contamination. The chamber should be designed for quick and thorough purging. The basic components of the gas chamber are illustrated in Figure 2.

[6]Kevlar is a trademark.

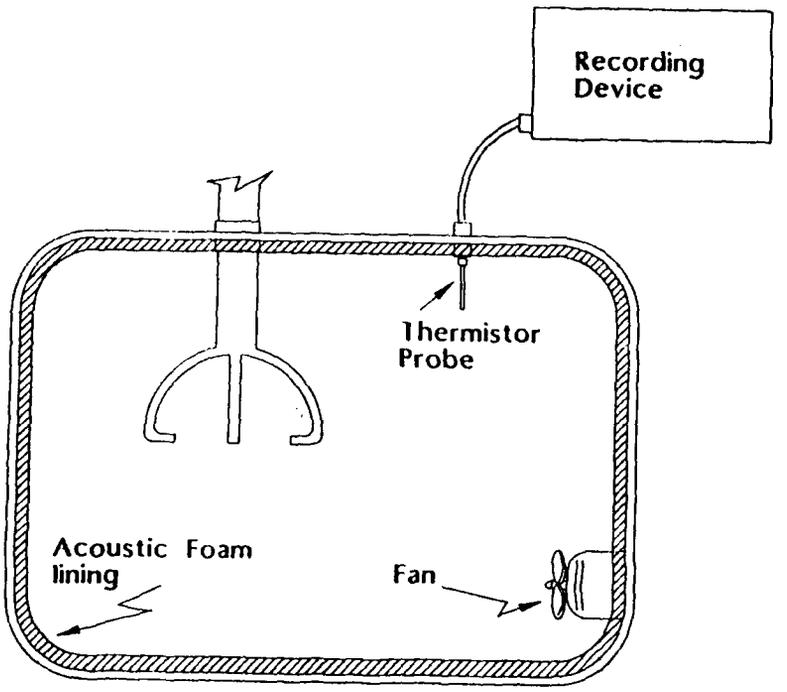

Figure 1. Sonic anemometer probe in a zero wind chamber.

6.2.2 Gas Source and Plumbing. Connect the pathlength chamber to two pressurized gas sources (nitrogen and argon) and use a purge pump to draw off expended gases. Required purity of the gas is 99.999%.

6.3 Temperature and Pressure Transducers. Each zero wind and pathlength chamber shall contain a temperature probe and a recording readout. Required temperature measurement precision is $\pm 0.2°C$.

6.4 Wind Tunnel:

6.4.1 Size. The wind tunnel shall be large enough to fit the entire instrument probe head along and cross axis plus sufficient clearance on each sidewall to prevent erroneous readings due to sidewall drag. The maximum projected area of the sonic head shall be less than 5 percent of the tunnel cross-sectional area.

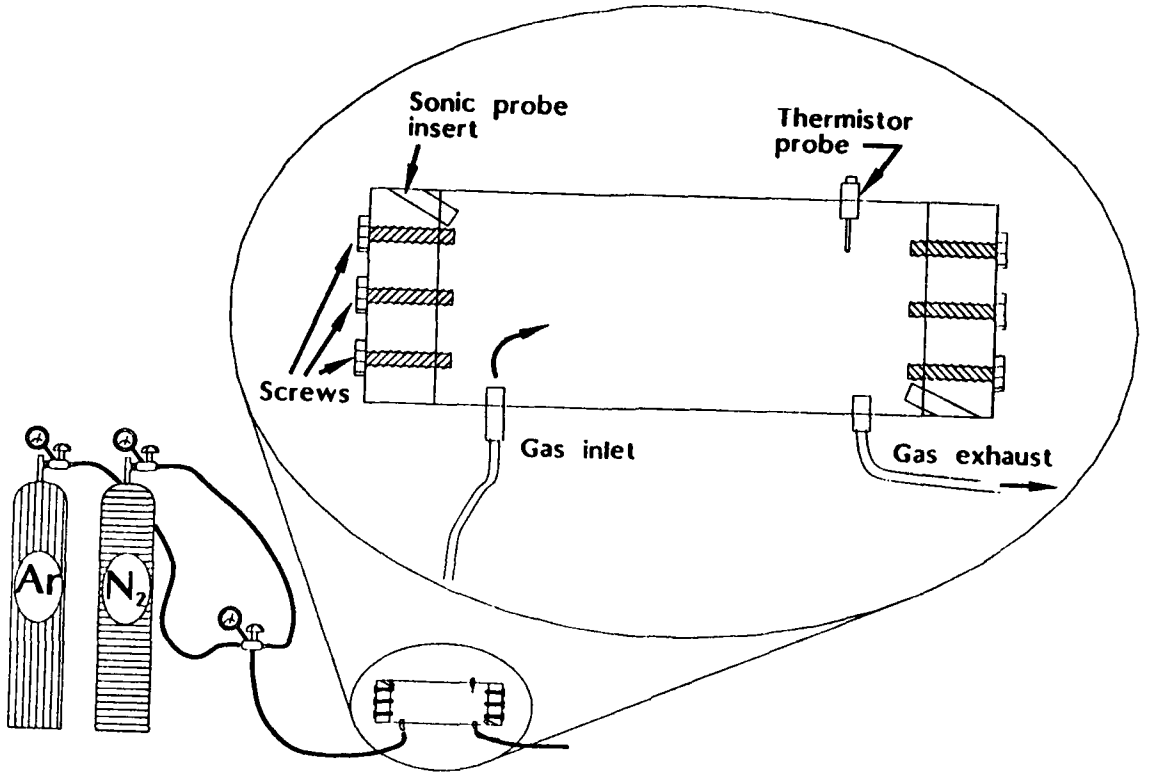

Figure 2. Pathlength chamber for acoustic pathlength determination.

6.4.2 Speed Range. The wind tunnel shall have a speed control that varies the flow rate over a range of at least 0.5 to 20 m/s. The speed control shall maintain the flow rate to within ±0.1 m/s.

6.4.3 Calibration. The mean flow rate shall be verified by use of transfer standards which have been calibrated by the National Institute of Standards and Technology (NIST) or by an equivalent fundamental physical method.

6.4.4 Turbulence. The wind tunnel shall have a uniform velocity profile and known turbulence scale and intensity throughout the test section.

6.5 Measuring System:

6.5.1 Counter. The digital counter used with the chambers shall be able to resolve counts equaling or exceeding the clock rate of the sonic anemometer/ thermometer.

6.5.2 Angle of Attack. Mount the sonic transducers on a rotating plate for wind tunnel transducer shadow trials. The plate rotation requirements are ±90 deg in the horizontal and ±30° in the vertical, with an angular resolution of 0.5 deg.

6.5.3 Recording Techniques. A recording system with at least a 10 Hz rate and a resolution comparable to the sonic instrument is required. Recording onto magnetic or optical media is recommended.

6.5.4 It is assumed that instruments tested by this method have adequate internal alignment and that the wind tunnel mounting apparatus has adequate tilt angle adjustment. Internal instrument alignment to within at least ±1 deg and apparatus tilt angle resolution to within ±0.1 deg or better are recommended for instruments used to provide means or variances. Internal alignment must be known to within ±0.1 deg for instruments used to provide measurements for momentum flux computations (6).

6.5.5. Calipers or a calibration jig with a tolerance of at least 1 mm are required to measure transducer spacing. For caliper measurements used as an alternative to pathlength chamber measurements of acoustic pathlength, caliper tolerance of 0.1 mm is required.

7. Precautions

7.1 Care must be exercised while using pressurized gases. Safety procedures

for the storage and handling of gas containers shall be posted and observed. Perform all testing with pressurized gases in a well ventilated room. Use of the "buddy system" is recommended.

7.2 Chamber temperatures and pressures should be stable and maintained close to laboratory temperature and pressure to minimize gradients that could cause convection within the chamber. However, sufficient pathlength chamber pressure and purge capability shall be maintained to prevent contamination from extraneous gases.

7.3 Ascertain that acoustic reflections are not contaminating results in pathlength chamber tests.

7.4 Ensure that the transducer geometry is not altered when mounted in the pathlength chamber.

7.5 Exercise care to minimize vibration and acoustic reflections in the wind tunnel test section during measurements.

7.6 It is assumed that the sonic anemometer array has sufficient rigidity and tensile strength to resist vibration and/or deformation over its operating range.

7.7 This method addresses only the performance of the sonic anemometer/thermometer. Operational use of this instrument requires the use of data collection, processing, and display equipment. The performance of such equipment is beyond the scope of this method.

8. Sampling

8.1 Acoustic Pathlength. If the pathlength chamber procedure is used, repeat the procedures used to determine acoustic pathlengths in argon and nitrogen gases for a minimum of 10 times, or until consistent results are achieved. If the caliper method is used, measure and verify transducer spacing to a tolerance of 0.1 mm before and after accomplishing the test procedure.

8.2 Thermal Stability Range. Obtain and verify a zero velocity reading at room temperature. If velocity shifts due to decalibration are noticed at selected higher or lower temperatures, repeat the measurements at these temperatures until consistent results are obtained.

8.3 Velocity Calibration Range. If a shift off calibration is observed, slowly adjust wind tunnel velocity with tunnel speed ascending and then descending to define U_c and U_s. Repeat the procedure until at least six consistent readings, three with wind speeds ascending and three with wind speeds descending, are obtained.

8.4 Transfer Function:

8.4.1 For orthogonal axis sonic anemometers, select a low velocity setting (near 2.0 m/s) and take one head on (0 degree) reading followed by one reading at each 10 degree interval to +90 degrees. Reverse the process, going back through 0 degrees to -90 degrees and return to 0 degrees (a total of 37 readings). Average the results to a single value for each angular position. Use a measurement period of 30 s at each angle, and begin measurements only when the tunnel velocity is stable at the selected velocity. Repeat the procedure for an intermediate velocity (5 to 6 m/s) and high velocity 10 m/s or greater, but not exceeding Us). Repeat the sequence for vertical angle

orientations of ±15° and ±30°.

8.4.2 For non-orthogonal axis sonic anemometers, follow sampling procedures described in (7).

9. Procedure

9.1 Increment of Resolution (Δv_i). Calculate the clock pulse resolution (Δt) as the inverse of the clock rate in Hz. Use a nominal speed of sound (340 m/s) and acoustic pathlength (d) to calculate a nominal transit time (t) between transducer pairs in a zero wind field. The increment of velocity resolution (Δv_i) is given by

$$\Delta v_i = \frac{d\ \Delta t}{2\ t^2} \qquad (6)$$

9.2 Standard Error of Velocity Estimate (Δv_n). It is assumed that errors in clock timing used to calculate Δv_i are randomly distributed and that the results of n velocity realizations are electronically averaged to produce each reported velocity reading. Determine the standard error of the velocity estimate by dividing Δv_i by the square root of n.

$$\Delta v_n = \Delta v_i / \sqrt{n} \qquad (7)$$

9.3 Acoustic Pathlength (d). Two different procedures are reported for defining d. One procedure uses a pathlength chamber with nitrogen and argon gases, while the other relies on precise transducer spacing measurements and a zero wind chamber. The pathlength chamber method has the advantage of well known thermodynamics constants for pure gases, but has the disadvantage of requiring extra equipment associated with the use of these gases. Also, small changes may occur in pathlength geometry when the chamber is clamped onto a set

of transducers. The transducer spacing measurement technique has no additional equipment requirements other than a set of calipers or a special jig with a measurement tolerance 0.1 mm. The disadvantage of this technique is the uncertainty in thermodynamics constants due to the variable composition of ambient air.

9.3.1 The Pathlength Chamber Method. Mount one axis of the anemometer array in a gas chamber, purge the chamber, and fill with nitrogen (N_2)gas. Check the seals for leaks. Record transit times t_1 and t_2 and chamber temperature (T,K). Use the NIST values for specific heat ratios ($\gamma = c_p/c_v$) and T to solve for speed of sound in nitrogen c_{N_2}

$$c_{N_2} = [\gamma f R^* T/M]^{0.5} \qquad (8)$$

where R^* is the universal gas constant (8314.34 $x10^4$ erg/mol/K), f is a compressibility factor (0.999972 for nitrogen and 0.99925 for argon),and M is the molecular weight (28.0134 for nitrogen and 39.948 for argon) **(8)**. Use the speed of sound for nitrogen and the t_1 and t_2 summations to solve for d. For n=20 summations and a 12-Mhz clock, d is determined by

$$d = 2c/((1/\Sigma t_1 + 1/\Sigma t_2)(n)(12)(10^6)) \qquad (9)$$

Repeat the procedure until a consistent sample is obtained. Purge the chamber, fill with Argon (Ar), and repeat the procedure. Calculate system delay (δt) using the averaged values of speed of sound and acoustic pathlength determined for N_2 and Ar. The delay in μs is given by

$$\delta t = \left| \frac{d_{N_2} - d_{Ar}}{c_{N_2} - c_{Ar}} \right| \qquad (10)$$

The delay time in μs multiplied by the clock rate ($12x10^6$) is a count number that is subtracted from counts in the system software or EEPROM. The electronic delay will remain the same for all transducer axes. The procedure is completed by verifying transducer spacing on each axis of the array to a tolerance of 1 mm.

9.3.2 The Transducer Spacing Method. Measure the transducer spacing on each axis of the array to a tolerance of 0.1 mm. Place the array in the zero wind chamber. Use dessicant in the chamber to control humidity. Use NIST values for specific heat of air at laboratory temperature and pressure to calculate the speed of sound in air.

$$c_{air} = [\gamma f R^* T_v / M]^{0.5} \qquad (11)$$

where M is the molecular weight of air and T_v is the virtual temperature. Nominal values of the thermodynamic constants for air and their uncertainties are provided in Table 1. Use the calculated speed of sound, clock time summations, and clock rate to define d as in section 9.3.1. System delay is the difference between the calculated d and caliper measurements.

Table 1. Nominal values for the universal gas constant (R^*), specific heat ratio (γ), compressibility factor (f), and molecular weight of dry air (M), and their respective uncertainties (2).

Variable	Units	Nominal Value	Uncertainty
R^*	10^4 erg/mol K	8314.36	±0.08
γ	dimensionless	1.40	±0.01
f	dimensionless	0.9997	±0.00005
M	g/mol	28.966	±0.02

9.4 Thermal Stability Range. Obtain a zero wind reading in the calibration chamber at room temperature. Lower the temperature of the chamber and acoustic array 20°C or to the coldest desired calibration temperature. Obtain a zero wind reading when the chamber and array temperature stabilizes. Velocity readings greater than two times the standard error of the velocity estimate indicate the presence of a temperature bias. Record the bias and repeat the procedure at progressively warmer temperatures until the bias is below the prescribed threshold. Warm the chamber to 20°C above room temperature or to the warmest desired calibration temperature and repeat the procedure.

9.5 Velocity Calibration Range. This procedure is designed to check for Reynolds number effects on the transducer drag coefficient (1). Orient the transducer array axis head on (0 deg) into the flow of a wind tunnel. Tunnel velocity is set at its lowest possible setting, or to achieve a Reynolds number near 100 for the transducer array. Note the ratio of tunnel velocity to anemometer velocity (v_t/v_d). Increase tunnel velocity 0.1 m/s and note any change in the v_t/v_d ratio. Repeat this procedure until consistent v_t/v_d ratios are achieved over a velocity range of 1.0 m/s. The velocity where the lowest

consistent v_t/v_d ratio is achieved is U_c. Note that determination of U_c may be limited by tunnel capabilities, whereupon the lowest achieveable tunnel velocity is used as an estimate of U_c. Increase tunnel velocity to a velocity corresponding to a transducer Reynolds number near 50,000. Note the v_t/v_d ratio and adjust the tunnel velocity up or down until a discontinuity or instability in v_d is observed. The highest velocity at which the v_t/v_d ratio remains stable is U_s, the upper end of the velocity calibration range.

9.6 Transducer Shadow Correction. This procedure is applicable to a representative sample of each sonic anemometer type or model designed for horizontal wind component measurement. The shadowing measurements will be made along horizontal axes for level (0-deg elevation) and at selected orientation angles with respect to the horizontal and vertical axes as described in Section 8.3. The wind tunnel measured velocity v_t multiplied by the cosine of the transducer axis orientation is the wind tunnel along-axis wind component ($v_{dm} = v_t \cos \Theta$). The mean wind component transfer function is presented as an equation or lookup table that describes v_{dm}/v_d as a function of Θ, v_t, and possibly turbulence scale and intensity.

9.7 Shadow Correction Check. With transducer shadow correction algorithm installed, repeat procedure 9.6 and note V_{dm}/V_d ratios. Report maximum deviations of V_{dm}/V_d from unity as measurement uncertainty.

9.8 Intercomparison Tests. These tests are conducted in fully turbulent flow. They are designed to verify the application of transfer functions derived in a wind tunnel to measurements in fully turbulent flow conditions.

9.8.1 Mount two sonic anemometers adjacent to each other on a stationary tower in accordance with the Standard Practice for Measuring Surface Wind and/or Temperature (ASTM DXXXX). Mount the arrays as close together as possible without inducing flow blockage or acoustic interference, and at 45° with respect to each other to maximize the differences in exposure of array geometry.

9.8.2 Obtain sets of 20-minute data runs under different wind speed and stability regimes.

9.8.3 Report intercomparison results in terms of bias, comparability, and precision for derived data. Note: The analysis of comparative spectra, if available, are recommended as a supplement to the bulk analysis results.

10. Report

10.1 Report the increment of resolution (m/s) and standard error of the velocity estimate (m/s).

10.2 Report the average acoustic pathlength (m) and system delay (μs). Include in the report the number of separate array axes used to determine these performance characteristics and the standard deviation of the results.

10.3 Report the velocity calibration range (m/s).

10.4 Report the thermal stability range (°C).

10.5 Report instrument intercomparison results in terms of bias, comparability, and precision (m/s).

11. Method Uncertainty

11.1 the contributions of temperature measurement and thermodynamic constant uncertainties to acoustic pathlength determination arise through the speed of sound equation. These uncertainties, expressed in percent of c, are presented in Table 2 for both the pathlength chamber method and the transducer spacing method. These figures were obtained with assumptions of a pressure near 1 kPa and temperature near 25°C. The assumed temperature measurement precision is ±0.2°C, with moisture controlled with dessicant for the transducer spacing method.

Table 2. Estimated Uncertainties in Speed of Sound c due to Uncertainties in M, γ, f, and T.

Type of Pathlength Determination	Uncertainty in c (%)			
	M	γ	f	T
Pathlength Chamber	0.01	0.1	0.01	0.03
Transducer Spacing	0.5	0.5	0.02	0.1

11.2 System delay affects velocity readings by increasing t_1 and t_2 in Equation 3 by a factor of δt, on the order of 10μs. This δt affects time by a factor of 0.43% per μs of delay, producing a comparable velocity error.

11.3 Transducer spacing measurement uncertainties affect velocity readings by a factor of δd in Equation 3. This creates a velocity error of 0.67% for each millimeter of error on a 15 cm path, and a 0.4% velocity error per millimeter of error on a 25 cm path. In practice, transducer spacing can vary by several tenths of a millimeter due to thermal expansion and wind loading

effects. Changing or adjusting transducers can generate even larger spacing differences.

12. References

(1) Ota, T., H. Nishiyama, Y. Taoka, 1987: Flow around an elliptic cylinder in the critical Reynolds number regime. J. Fluids Eng., 109, 149-155.

(2) List, R. J., 1958: Smithsonian Meteorological Tables. Smithsonian Institution, 527 pp.

(3) Coppin, P. A., and K. J. Taylor, 1983: A Three Component Sonic Anemometer/Thermometer System for General Micrometeorological Research. Boundary Layer Meteor., 27, 27-42.

(4) Horst, T. W., 1973: Spectral transfer functions for a three-component sonic anemometer, J. Appl. Meteor., 12, 1072-1075.

(5) Schotland, R. M., 1955: The measurement of wind velocity by sonic means. J. Meteor., 12, 386-390.

(6) Kaimal, J. C., and D. A. Haugen; 1969: Some Errors in the Measurement of Reynolds Stress, J. Appl. Meteor., 8, 460-462.

(7) Kraan, C., and W. A. Oost, 1989: A new way of anemometer calibration and its application to a sonic anemometer, J. Atmos. Oceanic Tech., 6, 516-524.

(8) Younglove, B. A., 1982: Thermophysical Properties of Fluids, I. NBS, Boulder, CO, 354 pp. Amer. Chem. Soc. Distribution Center, 1155 16th St., NW, Wash. DC 20036.

INTENTIONALLY BLANK

APPENDIX E: REFERENCES

ASTM, 1988: Standard practice for determing the operational comparability of meteorological measurements, D4430-84. Amer. Soc. For Testing and Materials, Philadelphia, PA pp. 330-332.

Baker, C. B., R. E. Eskridge, P. S. Conklin, and K. R. Knoerr, 1989: Wind tunnel investigation of three sonic anemometers (to be published as a NOAA Technical Memorandum circa Dec. 89).

Biltoft, C. A., 1987: Development of sonic anemometer software. Report No. DPG-FR-88-702, U.S. Army Dugway Proving Ground, Dugway, UT. AD:B120769.

Biltoft, C. A., 1988: Field Test of a Crosswind Scintillometer. Report No. DPG-FR-88-317, U.S. Army Dugway Proving Ground, Dugway, UT. AD:A200697.

Chintawongvanich, P., R. Olsen, and C. Biltoft, 1989: Intercomparison of Wind Measurements from Two Acoustic Doppler Sodars, a Laser Doppler Lidar, and In-Situ Sensors. J. Atmos. and Oceanic Tech., 6, 785-797.

Climet Instruments, Inc., 570 San Xavier Avenue, Sunnyvale, CA, April 1964.

Hanafusa, T., T. Fugitana, Y. Kobori, and Y. Mitsua, 1982: A new type sonic anemometer-thermometer for field operation. Pap. Meteorol. Geophys., 33, 1-19.

Hayashi, T., 1987: Dynamic response of a cup anemometer. J. Atmos. and Oceanic Tech., 4, 281-287.

Hoehne, W., 1971: Standardized Functional Tests. NOAA TM NWST&EL-12, U.S. Dept. of Commerce, Sterling, VA.

Hyson, P., 1972: Cup anemometer response to fluctuating wind speeds. J. Appl. Meteor., 11, 843-848.

Kaganov, E. 1., and A. M. Yaglom, 1976: Errors in wind-speed measurements by rotation anemometers. Boundary-Layer Meteor., 10, 15-34.

Kaimal, J. C., 1979: Sonic anemometer measurement of atmospheric turbulence. Proc. dynamic Flow conf., 1978. pp. 551-565. P.O. box 121, DK 2740 Skovlunde, Denmark.

Kaimal, J. C., and J. E. Gaynor, 1983: The Boulder Atmospheric Observatory. J. Climate and Appl. Meteor., 22, 863-880.

Kaimal, J. C., J. E. Gaynor, H. Zimmerman, and G. Zimmermann. Minimizing flow distortion errors in a sonic anemometer (draft paper submitted to Boundary Layer Meteorology).

Kondo, J., G. Naito, and Y. Fujinawa, 1971: Response of cup anemometer in turbulence. J. Meteor. Soc. Japan, 49, 63-74.

Lockhart, T. J., 1987: Anemometer performance determined by ASTM methods. J. Atmos. and Oceanic Tech., 4, 160-169.

MacCready, P. B., 1966: Mean wind speed measurements in turbulence. J. Appl. Meteor., 5, 219-225.

MacCready, P. B., and H. R. Jex, 1964: Response characteristics and meteorological utilization of propeller and vane wind sensors. J. Appl. Meteor., 3, 182-193.

Remtech, 1985: Remtech Doppler Sodar PDP 11/23 Operating Manual, Document No. 85/038A, Remtech, Inc., Avenue Del'Europe 78140 Velizy, France.

Silverman, B., 1968: The effect of spatial averaging on spectrum estimation. J. Appl. Meteor., 7, 168-172.

Snow, J. T., D. E. Lund, M. D. Conner, S. B. Harley, C. B. Pedigo, 1989: The dynamic response of a wind measuring system. J. Atmos. and Oceanic Tech., 6, 140-146.

Wyngaard, J. C., J. T. Bauman, and R. A. Lynch, 1974: Cup anemometer dynamics. Flow: Its Measurement and Control in Science and Industry, Vol. 1, R. B. Dowell, Ed. Instrument Society of America, 701-708.